Indonesian Journal of Science & Technology

Journal homepage: http://ejournal.upi.edu/index.php/ijost/

Towards Understanding the Corrosion Inhibition Mechanism of Green Imidazolium-Based Ionic Liquids for Mild Steel Protection in Acidic Environments

Elhachmia Ech-Chihbi[1,2], Fadoua EL Hajjaji[2], Abderrahim Titi[2], Mouslim Messali[3], Savas Kaya[4], Goncagül Serdaroğlu[5], Belkheir Hammouti[1], Mustapha Taleb[2]*

[1]Euro-Mediterranean University of Fes, Fez, Morocco
[2] Sidi Mohamed Ben Abdellah University, Fez, Morocco
[3]Imam Mohammad Ibn Saud Islamic University (IMSIU), Riyadh, Saudi Arabia
[4]Sivas Cumhuriyet University, Sivas, Turkey
[5]Cumhuriyet University, Sivas, Turkey

*Correspondence: E-mail: chahbi.elhachmia@gmail.com

ABSTRACT

Two novel ecological ionic-liquid derivatives based on imidazolium (ILs), namely, 3-(2-ethoxy-2-oxoethyl)-1-phenethyl-1H-imidazol-3-ium-chloride [OE-IM+, Cl-] and 3-(4-ethoxy-4-oxobutyl)-1-phenethyl-1H-imidazol-3-ium-chloride [OB-IM+, Cl-] was studied by Electrochemical Impedance Spectroscopy (EIS), Potentiodynamic Polarization (PP), SEM/EDX analysis and theoretical calculations. It is found that the studied ionic liquids exhibit high inhibition performance for Mild steel (MS) in 1 M HCl. Hence the formation of a barrier layer that retards redox reactions and therefore prevents the corrosion process of MS. Inhibition efficiency for all the compounds increases with their concentration and follows the order [OE-IM+, Cl-] < [OB-IM+, Cl-], indicating effective performance was achieved as the length of the alkyl chain attached to the imidazolium ring extended. Furthermore, DFT and MD simulations were used, revealing the impact of molecular configuration on the anticorrosive properties of these chemicals.

ARTICLE INFO

Article History:
Submitted/Received 01 Jan 2024
First Revised 18 Feb 2024
Accepted 10 Apr 2024
First Available online 16 Apr 2024
Publication Date 01 Sep 2024

Keyword:
Adsorption mechanism, Adsorption, Imidazolium-ILs, Morphology characterization, Protection.

© 2024 Tim Pengembang Jurnal UPI

1. INTRODUCTION

It is well known that pickling and acid cleaning are the processes most widely used in some industries to eliminate the products of corrosion deposited on metal surfaces (Boumhara *et al.*, 2015; Cris *et al.*, 2023; Sheetal *et al.*, 2024). Hydrochloric acid is one of the frequently used corrosive acid solutions. Nevertheless, these solutions are highly corrosive and can induce changes in many physicochemical characteristics of metals as a result of these industrial operations (Ech-chihbi *et al.*, 2016; Ghazoui *et al.*, 2013; Zerga *et al.*, 2010; Asmara *et al.*, 2018). Therefore, corrosion inhibitors are the most relatively economical method to preserve metallic materials against corrosion damage. Organic inhibitors possess several reactive sites for adsorption onto metal surfaces such as hetero atoms (N, O, S, and P), heterocyclic rings, and conjugated unsaturated bonds (Deng *et al.*, 2024; Njoku *et al.*, 2023). Thus, they can form a thin film that blocks direct exposure between acidic medium and MS samples (Haque *et al.*, 2021). These compounds should have the objective of being non-toxic and eco-friendly. Recently, ionic liquids (ILs) have attracted great attention in the field of corrosion protection. Ionic liquids (ILs) represent innovative compounds characterized by distinct attributes including negligible vapor pressure, rapid reaction kinetics, low toxicity, excellent selectivity, and environmentally benign properties (Gadioli *et al.*, 2024; Souza *et al.*, 2023; Asfour *et al.*, 2023; Rochdi *et al.*, 2014). However, a review of the literature shows the application of different ILs containing an “imidazole-moiety” in a variety of scientific fields, including some corrosion studies (El-Hajjaji *et al.*, 2020; Feng *et al.*, 2018; Ardakani *et al.*, 2020; Li *et al.*, 2023; El-Nagar *et al.*, 2024; Ghiaty *et al.*, 2024). Theoretical methods such as density functional theory (DFT) and molecular dynamics (MD) simulations are widely recognized for their accuracy in elucidating the electronic properties of selected chemicals and their tendency to interact with steel surfaces (Ettahiri *et al.*, 2023).

Imidazole compounds are widely studied for their effectiveness as metal corrosion inhibitors in various environments, due to their interesting properties. In particular, imidazole molecules exhibit higher capacities as electron donors and acceptors, which facilitates their adsorption on metal surfaces. In a study conducted by Bouayad *et al.* (2017), 1,3-diallyl-5-nitro-1H-benzo[d]imidazol-2(3H)-one demonstrated an impressive corrosion inhibition rate of approximately 90% when applied to protect mild steel in HCl solutions. However, when an imidazolium-based compound is bound to an ionic liquid, in this case 3-(4-phenoxybutyl)-1-propyl-1H-imidazol-3-ium bromide, the inhibition efficiency reaches over 94% (Zarrouk *et al.*, 2012).

This paper aims to investigate the inhibitory effects of two newly developed environmentally friendly derivatives of imidazolium-based ionic liquids on the corrosion of MS in 1 M HCl solution. Specifically, the compounds under examination are 3-(2-ethoxy-2-oxoethyl)-1-phenethyl-1H-imidazol-3-ium chloride [OE-IM+, Cl-] and 3-(4-ethoxy-4-oxobutyl)-1-phenethyl-1H-imidazol-3-ium chloride [OB-IM+, Cl-]. The assessment of both studied products as corrosion inhibitors involve electrochemical polarization, electrochemical impedance techniques, adsorption isotherms, computation of activation energy, and in-depth computational studies.

2. EXPERIMENTAL WORK

2.1. Synthesis Methodology of [OE-IM$^+$, Cl$^-$] and [OB-IM$^+$, Cl$^-$]

The synthesis procedure involved adding ethyl 2-chloroacetate and/or ethyl 4-chlorobutanoate (1.1 equivalents) to a solution of 1-phenethyl-1H-imidazole (1 equivalent) in toluene. The resulting solution underwent irradiation for 20 minutes in a closed vessel at 80°C

DOI: https://doi.org/10.17509/ijost.v9i2.68764
p- ISSN 2528-1410 e- ISSN 2527-8045

using a CEM Microwave. Completion of the reaction was evidenced by the formation of an oil phase from the initially clear homogeneous mixture of 1-phenethyl-1H-imidazole and the alkyl halide in toluene. The product was then extracted with ethyl acetate, followed by drying at reduced pressure. **Figure 1** illustrates the molecular structures of the imidazolium-based ionic liquids studied. The synthesis of these ionic liquids (ILs) was conducted at the Chemistry Department, Faculty of Science, Taibah University, located in Al-Madinah Al-Mounawwara, Saudi Arabia.

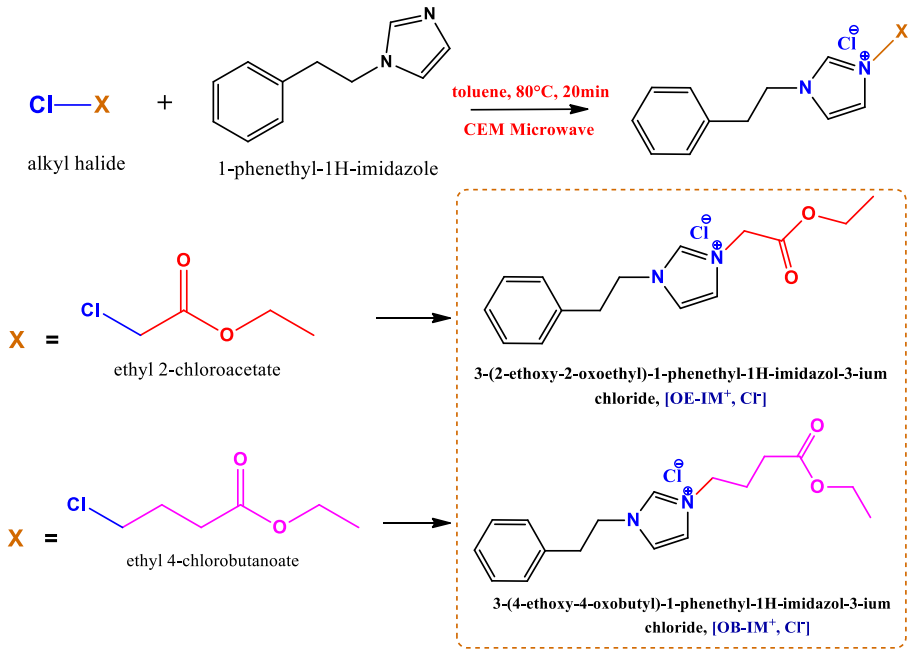

Figure 1. Procedure to Synthesize [OE-IM+, Cl-] and [OB-IM+, Cl-] inhibitors.

2.2. Characterization of [OE-IM$^+$, Cl$^-$] and [OB-IM$^+$, Cl$^-$]

[OE-IM+, Cl-]: FT-IR, cm^{-1}: = 756 (C-H, CH2), 1021 (C-O), 1225 (C-N), 1560 (C=N), 1747 (C=O), and 2910 and 3100 (Ar-H). 1H NMR (400 MHz, CDCl3): δH = 1,17 (t, 3H CH3), 3,11 (t, 2H, CH2), 4,12 (qd, 2H, CH3), 4.46 (t, 2H, CH2), 5,29 (s, 2H, CH2), 7,1–7,54 (d, 2H, Ar-H), 7.05–7.30 (m, 5H, Ar-H), and 8,18 (s, 1H, Ar-H); 13C NMR (100 MHz, CDCl3): δC = 13,85 (CH3), 36,4 (CH2), 50,1 (CH2), 62,7 (CH2), 122.1 (CH), 123.54 (CH), 127,33 (CH), 128,9 (CH), 135,7 (C), 137,8 (CH), and 166,1 (CO); Found: C, 61.20, H, 6.43, N, 9.61%. Calcd. for C15H19ClN2O2, C, 61.12, H, 6.50, N, 9.50%.

[OB-IM+, Cl-]: FT-IR, cm^{-1}: = 747 (C-H, CH2), 1021 (C-O), 1154 (C-N), 1561 (C=N), 1728 (C=O), and 2910 and 3100 (Ar-H). 1H NMR (400 MHz, CDCl3): δH = 1.19 (3H, CH3), 2.26 (quint, 2H, CH2), 3.18 (t, 2H, CH2), 4.06 (q, 2H, CH3), 4.30 (t, 2H, CH2), 4.56 (t, 2H, CH2), 7.15–7.43 (d, 2H, Ar-H), 7.05–7.34 (m, 5H, Ar-H), and 10.12 (s, 1H, Ar-H); 13C NMR (100 MHz, CDCl3): δC = 14.1 (CH3), 25.5 (CH2), 30.3 (CH2), 36.4 (CH2), 48.8 (CH2), 51.0 (CH2), 60.8 (CH2), 121.9 (CH), 121.9 (CH), 122.4 (CH), 127.4 (CH), 128.7 (CH), 128.9 (CH), 135.8 (CH), 122.4 (CH), 137.2 (CH), and 172.1 (CO); Found: C, 63.33, H, 7.11, N, 8.76%. Calcd. for C17H23ClN2O2, C, 63.25, H, 7.18, N, 8.68%.

2.3. MS and Solutions Preparation

The MS specimens utilized in the electrochemical and surface tests consisted of carbon (0.21 wt%), manganese (0.05 wt%), silicon (0.38 wt%), aluminum (0.01 wt%), phosphorus (0.09 wt%), with the remainder being iron. Before each test, the MS samples underwent

DOI: https://doi.org/10.17509/ijost.v9i2.68764
p- ISSN 2528-1410 e- ISSN 2527-8045

abrasion with wet abrasive paper ranging from grade 180 to 1500, followed by rinsing with distilled water and methanol, respectively, and subsequent drying for use. In this study, the corrosion inhibitors were directly dissolved in the aggressive solution without the use of any solvent. The corrosive electrolyte comprised a 1 M HCl solution prepared by diluting 37% HCl (reagent grade) with distilled water. Concentrations of the investigated imidazolium-based ionic liquids ranged from 10^{-6} to 10^{-3}M.

2.4. Electrochemical Measurements

Electrochemical measurements were conducted in a three-electrode cell containing 50 mL of the test solution, with MS serving as the working electrode (WE), Ag/AgCl as the reference electrode (RE), and Pt as the auxiliary electrode (AE). The MS coupons utilized had an exposed surface area of 1 cm^2. Before each measurement, the steel surface was immersed in the corrosive solution for half an hour to achieve a stable value of the open circuit potential (OCP). Subsequently, electrochemical impedance spectroscopy (EIS) was performed at the open circuit potential (E_{OCP}) across a frequency range of 100 kHz to 100 mHz, with an amplitude perturbation of 10 mV. The inhibition efficiency can be calculated from EIS tests using Equation (1) (Lazrak *et al.*, 2022; Salim *et al.*, 2021; Ben Hmamou *et al.*, 2015; Ech-chihbi *et al.*, 2023):

$$\eta_{EIS} = \frac{R_{P(inh)} - R_{P(blank)}}{R_{P(inh)}} \times 100 \quad (1)$$

where $R_{P(blank)}$ and $R_{P(inh)}$ denote the polarization resistance in the absence (blank) and presence of the examined ILs, respectively.

However, Tafel potentiodynamic polarization techniques were conducted over a range from -250 to +250 mV versus the OCP, employing a scanning speed of 0.5 mV/s. The inhibition efficiency utilizing this technique can be determined according to Equation (2) (El-Hajjaji *et al.*, 2020):

$$\eta_{PDP} = \frac{i_{corr(blank)} - i_{corr(inh)}}{i_{corr,blank}} \times 100 \quad (2)$$

where $i_{corr(blank)}$ and $i_{corr(inh)}$ refer to the current density before (blank) and after adding the inhibitor, respectively.

2.5. Surface Characterization

To investigate surface morphology, MS samples were immersed in 1 M HCl without any inhibitor (blank) and in the presence of [OE-IM^+, Cl^-] and [OB-IM^+, Cl^-] at 298K for 6 hours. SEM micrographs were captured using a Quattro ESEM-FEG equipped with X-ray photoelectron spectroscopy (EDX) analysis, operated at an accelerating voltage of 20 kV with a magnification of ×1000.

2.6. Computational Details

2.6.1. DFT computations

[OB-IM^+, Cl^-] and [OE-IM^+, Cl^-] compounds were optimized at the B3LYP/6311G (df, pd) level, by utilizing the G09W package program. The geometry of each compound was verified by the absence of a negative frequency, in both the gas and water media. The C-PCM (conductor-like polarizable continuum model) was used to perform all DFT calculations in the water phase. As known well from Koopmans Theorem, the ionization energy (I) can be estimated as the negative value of the HOMO energy, while the electron affinity (A) can be

DOI: https://doi.org/10.17509/ijost.v9i2.68764
p- ISSN 2528-1410 e- ISSN 2527-8045

approximated as the negative value of the LUMO energy. Based on the DFT theory, global reactivity descriptors, electronegativity (χ), chemical hardness (η), chemical potential (μ), and softness (σ) are defined as presented in Equations (3) & (4) (Mangalam *et al.*, 2021; Singh *et al.*, 2021):

$$\mu = -\chi = \left[\frac{\partial E}{\partial N}\right]_{v(r)} = -\left(\frac{I+A}{2}\right) \tag{3}$$

$$\eta = \frac{1}{2}\left[\frac{\partial^2 E}{\partial N^2}\right]_{v(r)} = \frac{I-A}{2} \tag{4}$$

$$\sigma = 1/\eta$$

Here, *E* is the total electronic energy, and *N* is the number of electrons. In addition, Parr and co-workers (Parr *et al.*, 1999) have defined the electrophilicity index. Subsequently, Chattaraj introduced the concept of nucleophilicity (ε) as the reciprocal of the electrophilicity index, as depicted in Equations (5) & (6):

$$\omega = \chi^2 / 2\eta = \mu^2 / 2\eta \tag{5}$$

$$\varepsilon = 1/\omega \tag{6}$$

Two new parameters, termed electron-donating power (ω^-) and electron-accepting power (ω^+), providing useful information about electron donating and accepting abilities have been proposed by Gazquez and coworkers (Gazquez *et al.*, 2007). These descriptors, derived from the ground-state ionization energy and electron affinities of molecules, are outlined following Equations (7) & (8):

$$\omega^+ = (I+3A)^2 / (16(I-A)) \tag{7}$$

$$\omega^- = (3I+A)^2 / (16(I-A)) \tag{8}$$

The dipole moment (*DM*) and linear polarizability (α) values, contingent upon the *x*, *y*, and *z* components within the "Cartesian coordinate system", are expressed following Equations (9) & (10):

$$DM = (\mu_x^{\,2} + \mu_y^{\,2} + \mu_z^{\,2})^{1/2} \tag{9}$$

$$\langle\alpha\rangle = 1/3\left[\alpha_{xx} + \alpha_{yy} + \alpha_{zz}\right] \tag{10}$$

The determination of the fraction of electrons transferred between the metal surface and the inhibitor molecule, along with the metal-inhibitor interaction energy, are crucial parameters in predicting the corrosion inhibition efficacy of molecules. The formulations of Equations (11) & (12) concerning these parameters have been derived following the principles of Electronegativity Equalization and Hardness Equalization (Serdaroğlu *et al.*, 2020).

$$\Delta N = \frac{\phi_{Fe} - \chi_{inh}}{2(\eta_{Fe} + \eta_{inh})} \tag{11}$$

$$\Delta\psi = -\frac{(\phi_{Fe} - \chi_{inh})^2}{4(\eta_{Fe} + \eta_{inh})} \tag{12}$$

DOI: https://doi.org/10.17509/ijost.v9i2.68764
p- ISSN 2528-1410 e- ISSN 2527-8045

In this context, Φ_{Fe} and η_{Fe} denote the work function and absolute hardness of the metal, respectively, set at 4.82 and 0.0 eV/mol. Similarly, χ_{inh} and η_{inh} represent the electronegativity and hardness values of the inhibitor molecule, respectively. The optimized structure and results of surface analyses were visualized using the Gauss-view 6.0.16 package. The corrosion inhibition potential of [OE-IM$^+$, Cl$^-$] and [OB-IM$^+$, Cl$^-$] was assessed through B3LYP/6-311G (df, pd) level calculations in water using the C-PCM model, alongside gas-phase calculations.

2.6.2. Molecular dynamic calculations

For a deeper understanding of the atomic scale, molecular dynamics calculations were conducted under solvation conditions using a solution composition of 100 H_2O + 4 Cl^- + 3 H_3O^+. The simulation was carried out within a simulation box measuring 22 x 22 x 82 Å, comprising 7 Fe (110) layers with 10 x 10 Fe atoms per face and a vacuum region of 70 Å. The temperature of the systems under study was maintained at 298 K using Andersen's thermostat (Kumari *et al.*, 2017). A simulation time of 250 ps was chosen with a time step of 1 fs. All calculations were performed under periodic boundary conditions and utilized the COMPASS force field (El Faydy *et al.*, 2018). Electrostatic interactions were computed employing the Ewald method, whereas Van der Waals interactions were calculated through atom-based summation, as described in Equations (13) and & (14) (Benbouguerra *et al.*, 2018; Ouakki *et al.*, 2021).

$$E_{ads} = E_{total} - (E_{solution+metal} + E_{inhibitor}) \quad (13)$$

$$E_{binding} = -E_{ads} \quad (14)$$

where E_{total} is the total energy of the system, $E_{solution+metal}$ represents the total energy of the system without the inhibitor molecule, and $E_{inhibitor}$ stands for the energy of the inhibitor molecule.

3. RESULTS AND DISCUSSION

3.1. EIS Measurements

The electrochemical impedance diagrams illustrating the behavior of MS in molar hydrochloric acid medium at different concentrations are depicted in **Figure 2**. All EIS diagrams show one single depressed capacitive semi-circle, implying that the charge transfer mostly checked the corrosion process of the steel surface (Ansari *et al.*, 2018).

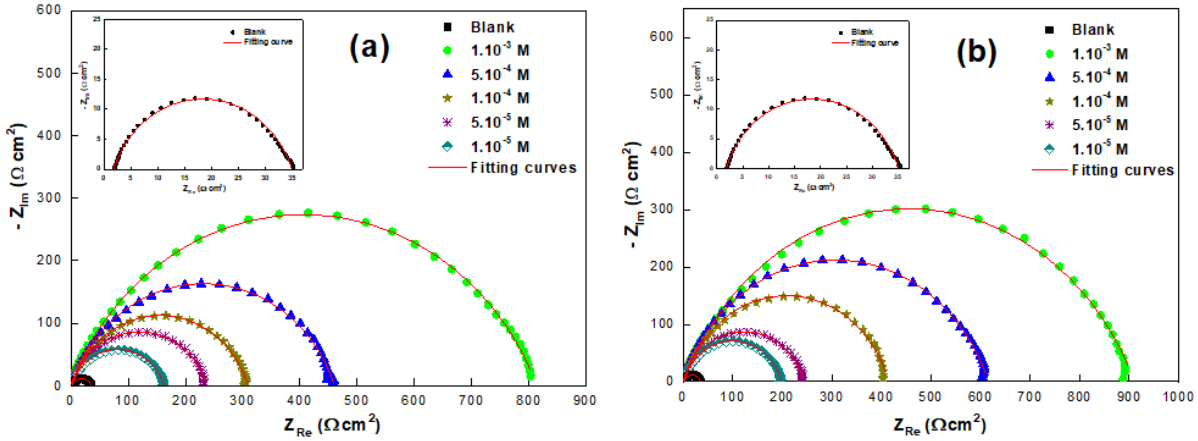

Figure 2. EIS diagrams for MS in 1 M HCl solution at 298K with varying concentrations of **(a)** : [OE-IM$^+$, Cl$^-$] and **(b)** : [OB-IM$^+$, Cl$^-$].

DOI: https://doi.org/10.17509/ijost.v9i2.68764
p- ISSN 2528-1410 e- ISSN 2527-8045

In addition, the size of the capacitive loops increased with the addition of [OE-IM$^+$, Cl$^-$] and [OB-IM$^+$, Cl$^-$] and expanded with increasing inhibitor concentration. These results confirm that these organic species have good inhibitory behavior due to their adsorption onto the MS surface (Ji *et al.*, 2016). The presence of depressed semicircles can be attributed to the roughness and heterogeneity of the active sites on the surface of MS (Ansari *et al.*, 2018).

Bode and phase angle plots were also executed and presented in **Figure 3**. For both tested compounds, the phase angle values are greater than those of the blank solution, but less than -90°, revealing that the capacitor is less than ideal. Meanwhile, only one peak in the phase angle diagram revealed that there was only a one-time constant occurring at the MS/electrolyte interface (Olivares *et al.*, 2007). A constant phase element (CPE) was employed to address deviations from the ideal frequency response, which is generally attributed to factors such as distributed surface reactivity, surface inhomogeneity, roughness, fractal geometry, electrode porosity, and other related characteristics (Rajeswari *et al.*, 2014). **Figure 4** displays the Electrical equivalent circuit (EEC) used to fit EIS data. This EC is constituted of *Rs* as solution resistance, R_P as polarization resistance, and CPE_{dl} as a Constant Phase Element. The expression delineating the impedance of the Constant Phase Element (CPE) is as follows, denoted by Equation (15) (Ech-chihbi *et al.*, 2023):

$$Z_{CPE} = \left[Q(j\omega)^n \right]^{-1} \tag{15}$$

where Q represents the magnitude of the CPE, ω is the angular frequency and $i^2 = -1$ denotes an imaginary number. n represents a deviation parameter, where $n = +1$ generally indicates a pure capacitor. The EIS parameters recorded by utilizing the selected EC are listed in **Table 1**.

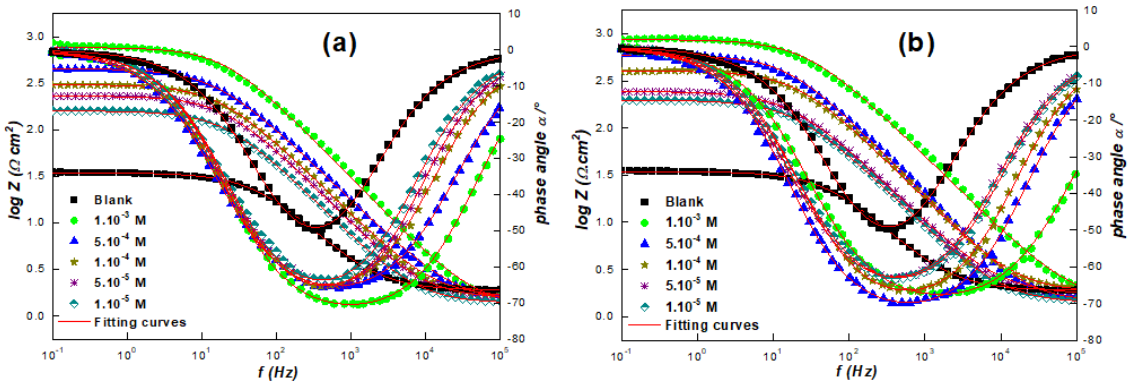

Figure 3. Bode plots for MS in 1 M HCl solution at 298K with various concentrations of **(a) :** [OE-IM$^+$, Cl$^-$] and **(b) :** [OB-IM$^+$, Cl$^-$].

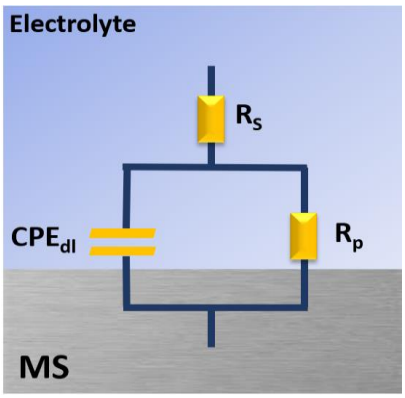

Figure 4. EEC used to fit the EIS data.

DOI: https://doi.org/10.17509/ijost.v9i2.68764
p- ISSN 2528-1410 e- ISSN 2527-8045

As shown in **Table 1**, the values obtained of the polarization resistance values are continuously improved and increase with the increasing concentration of [OE-IM$^+$, Cl$^-$] & [OB-IM$^+$, Cl$^-$]. on the other hand, the values of C_{dl} showed a significant decrease. This is probably caused by the due to changes occurring at the MS/HCl interface by a significant expansion of the thickness of the electric double-layer as a result of the adsorption of many organic molecules onto the MS surface (Zhang *et al.*, 2019). The percentage of EIS efficiency (η_{EIS}%) demonstrates an increase as the inhibitor concentration rises, reaching maximum values of 95.9% and 96.3% for [OE-IM$^+$, Cl$^-$] and [OB-IM$^+$, Cl$^-$] at 1.10^{-3} M, respectively. This finding can be attributed to a larger fraction of surface coverage at higher concentration levels.

Table 1. EIS parameters derived from nyquist diagram for blank solution (1 M HCl) and various concentrations of investigated ILs.

Medium	*Conc. (M)*	R_s *(Ω.cm²)*	R_P *(Ω.cm²)*	CPE_{dl}		n_{dl}	η_{EIS} *%*	*Θ*
				C_{dl} *(μF.cm^{-2})*	*Q (μF.S^{n-1})*			
Blank	--	1.7	33	89.1	312.70	0.784	**--**	--
[OE-IM$^+$, Cl$^-$]	1. 10^{-5}	1.4	161.6	48.7	129.1	0.798	**79.5**	0.795
	5. 10^{-5}	1.7	235.6	34.6	87.2	0.808	**85.9**	0.859
	1. 10^{-4}	1.5	307.5	28.7	72.2	0.805	**89.2**	0.892
	5. 10^{-4}	1.3	459.0	22.0	57.8	0.789	**92.8**	0.928
	1. 10^{-3}	1.2	815.4	11.9	37.4	0.753	**95.9**	0.959
[OB-IM$^+$, Cl$^-$]	1. 10^{-5}	1.4	197.3	40.4	107.8	0.797	**83.2**	0.832
	5. 10^{-5}	1.7	242.6	36.8	97.0	0.794	**86.4**	0.864
	1. 10^{-4}	2.3	412.4	20.9	57.8	0.810	**91.9**	0.919
	5. 10^{-4}	1.3	616.5	19.0	53.2	0.769	**94.6**	0.946
	1. 10^{-3}	1.1	909.1	7.6	26.8	0.746	**96.3**	0.963

3.2. Adsorption Isotherm Study

The information derived from the results of the EIS data was compared to different adsorption-isotherms to acquire crucial insights into the activity of the organic chemicals with the MS/corrosive solution interface. **Figure 5** presents the Langmuir adsorption isotherm plot at 298 K. The Langmuir isotherm can be described as indicated in Eq. (16) (Abdelshafi *et al.*, 2024; El-khlifi *et al.*, 2024):

$$\frac{C_{inh}}{\theta} = \frac{1}{K_{ads}} + C_{inh} \tag{16}$$

where C_{inh} represents the concentration of the investigated products, θ is assigned to the fraction of the surface coverage by the inhibitor (degree of coverage) and K stands for the adsorption equilibrium constant (L/mol).

In this study, the Langmuir model was selected as giving the best adjustment as shown in **Figure 5**. C_{inh}/θ versus C_{inh} (**Figure 5**) reveals linear relationships with slopes and regression coefficients (R^2) close to unity (**Table 2**). This strongly indicates that adsorption on the MS surface conforms well to this particular isotherm model. K_{ads} are linked to the standard free-energy-of-adsorption (ΔG_{ads}) as shown in Equations (17) & (18) (Goyal *et al.*, 2020; Azgaou *et al.*, 2022; Udunwa *et al.*, 2024).

$$K = 1/\text{intercept} \tag{17}$$

$$\Delta G_{ads} = -RT\, ln(55.5K) \tag{18}$$

DOI: https://doi.org/10.17509/ijost.v9i2.68764
p- ISSN 2528-1410 e- ISSN 2527-8045

Here, *T* represents the absolute temperature, and *R* denotes the universal gas constant. 55.5 represents the molar concentration of water. The computed adsorption parameters are summarized in **Table 2**.

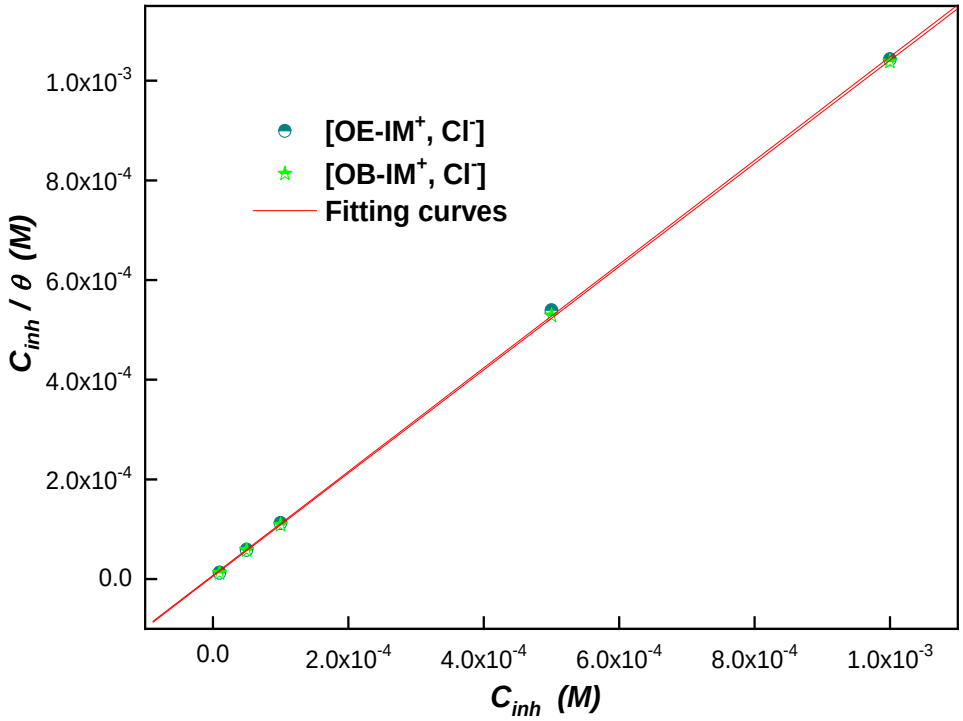

Figure 5. Langmuir adsorption isotherm plot for [OE-IM$^+$, Cl$^-$] and [OB-IM$^+$, Cl$^-$].

Table 2. Adsorption parameters of the [OE-IM$^+$, Cl$^-$] and [OB-IM$^+$, Cl$^-$].

Compound	R^2	Slopes	K ($L.mol^{-1}$)	ΔG_{ads} ($kJ.mol^{-1}$)
[OE-IM$^+$, Cl$^-$]	0.99988	1.04	13.7 10^4	-39.2
[OB-IM$^+$, Cl$^-$]	0.99997	1.03	19.2 10^4	-40.0

As depicted in **Table 2**, the computed values of ΔG_{ads} for [OE-IM$^+$, Cl$^-$] and [OB-IM$^+$, Cl$^-$] are around −40 kJ/mol (Azgaou *et al.*, 2022). This finding means that the adsorption process of the examined products to the MS surface is chemisorption, i.e. the adsorption process by the interaction of donor-acceptor active centers that exist on these inhibitor molecules and iron surface. The heteroatoms and delocalized sp^2 electrons on [OE-IM$^+$, Cl$^-$] and [OB-IM$^+$, Cl$^-$] inhibit the active centers on the surface of steel and retard the dissolution processes resulting in improvement in the inhibition of the metal surface.

3.3. Effect of Immersion Time

Figure 6 depicts the impedance diagrams for MS in molar hydrochloric acid solution in the presence of 10^{-3} M of [OE-IM$^+$, Cl$^-$] and [OB-IM$^+$, Cl$^-$] at various immersion durations (1/2 h to 12h). Analysis indicated that all EIS graphs exhibited a single capacitance loop, with their diameters decreasing over time. **Table 3** compiles the EIS parameters extracted from the Nyquist plots. The Nyquist spectra displayed a depressed semi-circular shape after the addition of inhibitors during the immersion period, indicating the predominance of a charge transfer process in MS corrosion. The equivalent electric circuit shown in **Figure 4** was used to fit the obtained data. However, further evaluation of the time behavior of the inhibitor is indicated, particularly concerning the kinetics associated with prolonged immersion times.

DOI: https://doi.org/10.17509/ijost.v9i2.68764
p- ISSN 2528-1410 e- ISSN 2527-8045

Analysis of **Table 3** reveals a decrease in R_P with immersion time, accompanied by an increase in C_{dl} values.

This evolution of R_P and C_{dl} can be attributed to the accelerated rate of iron dissolution, leading to the desorption of IL molecules from the steel surface (Hrimla *et al.*, 2021). The analysis also indicates slight variations over time, which do not significantly affect the efficiency values. Furthermore, the elevated values, reaching 96% at the end of the immersion test, confirm the stability of the film of adsorbed inhibitors in the acid solution.

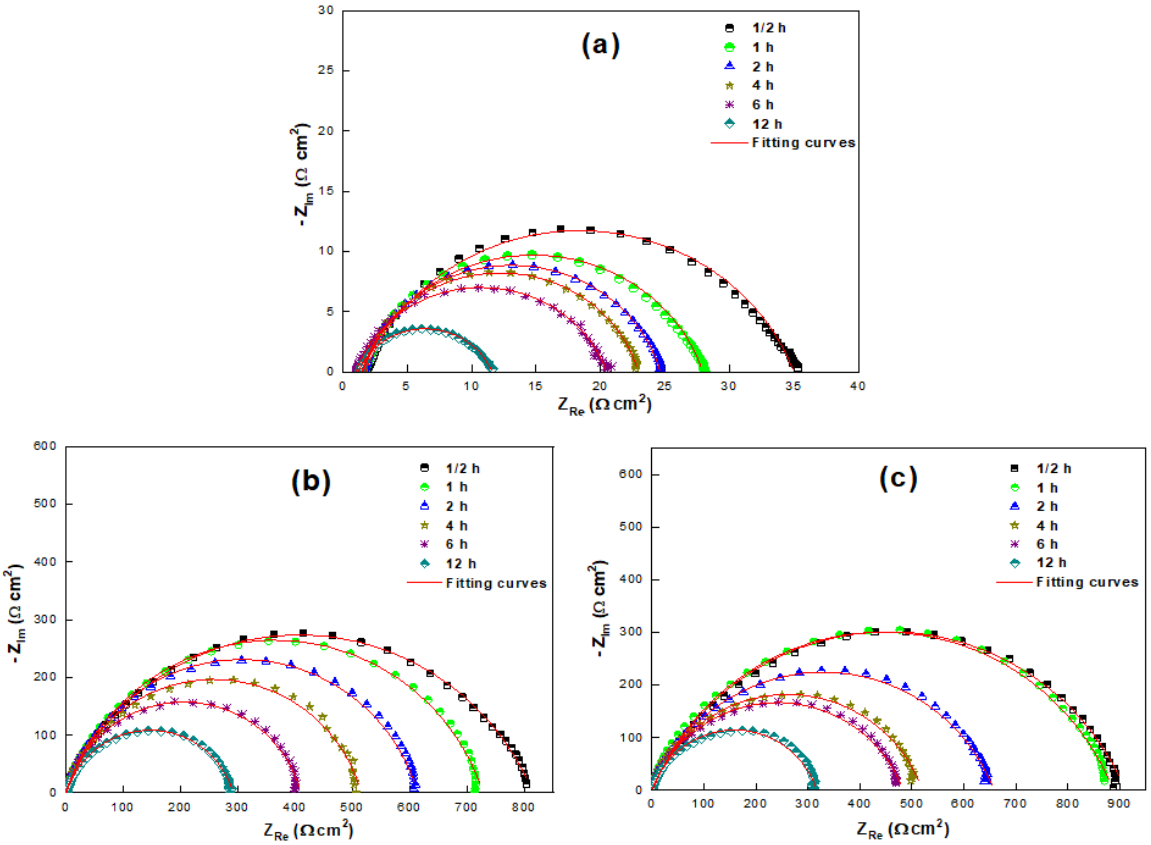

Figure 6. EIS Plots of MS in 1 M HCl **(a)** without and with 10^{-3}M of **(b)** [OE-IM$^+$, Cl$^-$] and **(c)** [OB-IM$^+$, Cl$^-$] at various immersion durations.

Table 3. Electrochemical parameters for MS in 1 M HCl before (Blank) and after adding both examined ILs at various time intervals.

Medium	*Time (h)*	R_s *(Ω.cm²)*	CPE_{dl}		C_{dl} *(μF/cm²)*	R_P *(Ω.cm²)*	η_{imp} *%*
			n_{dl}	Q *(μF.S^{n-1})*			
Blank	½	1.7	0.784	312.70	89.1	33.0	--
	1	1.6	0.810	364.90	122.7	26.4	--
	2	1.5	0.835	433.0	174.3	23.0	--
	4	1.5	0.834	627.00	267.0	21.4	--
	6	1.0	0.796	963.80	349.4	19.4	--
	12	1.2	0.764	949.20	419.5	10.4	--
[OE-IM$^+$, Cl$^-$]	½	1.2	0.753	37.4	11.9	815.4	**95.9**
	1	1.3	0.803	68.2	25.7	726.6	**96.3**
	2	1.1	0.824	75.8	32.5	612.5	**95.7**
	4	1.7	0.834	82.4	41.4	512.0	**95.8**
	6	1.5	0.839	92.7	50.2	408.3	**95.2**
	12	1.5	0.820	162.6	65.6	290.4	**96.4**

DOI: https://doi.org/10.17509/ijost.v9i2.68764
p- ISSN 2528-1410 e- ISSN 2527-8045

Table 3 (Continue). Electrochemical parameters for MS in 1 M HCl before (Blank) and after adding both examined ILs at various time intervals.

Medium	Time (h)	R_s ($\Omega.cm^2$)	CPE_{dl}		C_{dl} ($\mu F/cm^2$)	R_P ($\Omega.cm^2$)	η_{imp} %
			n_{dl}	Q ($\mu F.S^{n-1}$)			
[OB-IM$^+$, Cl$^-$]	½	1.1	0.746	26.8	7.6	909.1	**96.3**
	1	1.0	0.762	38.3	11.7	886.2	**97.0**
	2	0.9	0.765	40.7	12.4	657.4	**96.5**
	4	1.2	0.779	45.8	15.0	519.3	**95.8**
	6	0.8	0.770	50.4	22.5	483.0	**95.9**
	12	1.3	0.800	57.3	30.9	315.5	**96.7**

3.4. Polarization Plots

3.4.1. Effect of ILs concentration

The polarization plots of the MS in 1 M HCl before and after adding examined ILs at 298 K are graphically displayed in **Figure 7**. The current density values (i_{corr}) in both the cathodic and anodic segments of the polarization plots decrease in the presence of [OE-IM$^+$, Cl$^-$] and [OB-IM$^+$, Cl$^-$] compared to the uninhibited solution, and decrease further with the increase in the concentration, implying more efficient inhibitory behavior. This is due to the adsorption of these molecules that reduce both anodic iron dissolution and cathodic (reduction of proton ions) reactions. After the applied potential reached desorption potential (−250 mV), organic species desorbed from the MS surface and the inhibitors did not possess the capacity of corrosion inhibition (Hrimla *et al.*, 2021; Hamani *et al.*, 2014). **Table 4** presents the numerical values of electrochemical parameters such as corrosion current density (i_{corr}), Tafel cathodic slope (β_c), and corrosion potential (E_{corr}), as determined.

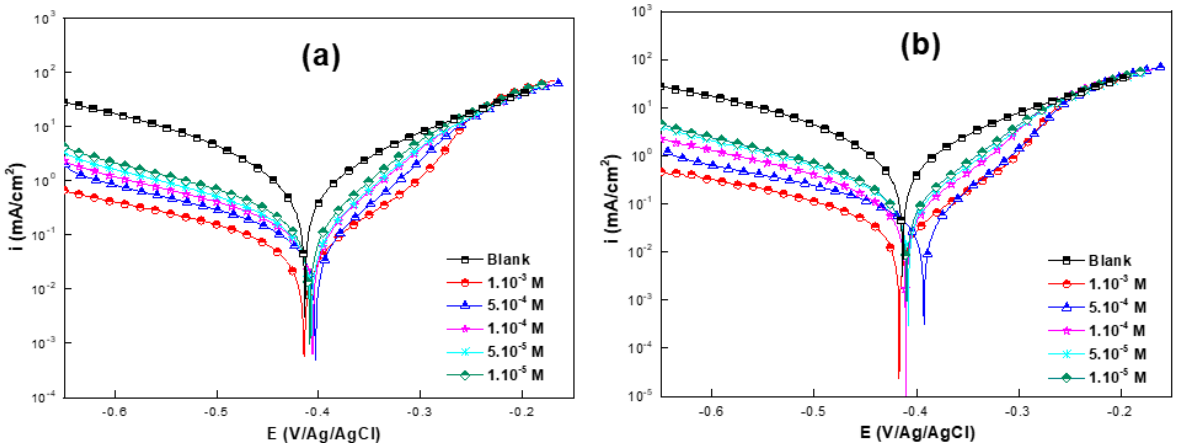

Figure 7. PDP plots for MS before and after adding different concentrations of **(a)** [OE-IM$^+$, Cl$^-$] & **(b)** [OB-IM$^+$, Cl$^-$] in 1 M HCl solution at 298 K.

For the blank (uninhibited medium), the value of i_{corr} was 944 µA/cm^2, while the values of i_{corr} for [OE-IM$^+$, Cl$^-$] and [OB-IM$^+$, Cl$^-$] decreased to 36 and 30 µA/cm^2, respectively. This finding meant both the studied ionic liquids can inhibit the corrosion process at the MS/electrolyte interface. Meanwhile, slight variations in the β_c values suggest that the proton evolution reaction was governed by an activation process, and the inclusion of both inhibitors did not influence the mechanism of hydrogen evolution. As depicted in **Figure 7** and **Table 4**, the E_{corr} values show no significant shift after the addition of [OE-IM$^+$, Cl$^-$] and [OB-IM$^+$, Cl$^-$]. Inhibitors are commonly classified as either anodic or cathodic inhibitors if the change in E_{corr} exceeds 85 mV (Ouakki *et al.*, 2020; Jalab *et al.*, 2023; Huang *et al.*, 2022). In the present

DOI: https://doi.org/10.17509/ijost.v9i2.68764
p- ISSN 2528-1410 e- ISSN 2527-8045

investigation, the shift of E_{corr} is less than 85 mV compared to the uninhibited medium, which indicates that both investigated products are considered "mixed-type inhibitors". In addition, the inhibitory effectiveness rises sharply with the concentration of both examined ILs, reaching maximum inhibition at 10^{-3} M (96% for both inhibitors).

Table 4. PDP parameters for MS corrosion in 1 M HCl solution in the absence and presence of various concentrations of the examined compounds.

Medium	Conc. (M)	$-\beta_c$ (mV/dec)	$-E_{corr}$ (mV/Ag/AgCl)	i_{corr} ($\mu A/cm^2$)	η_{PDP} (%)
Blank	--	139	413	944	--
[OE-IM$^+$, Cl$^-$]	10^{-5}	125	409	187	***80.1***
	5. 10^{-5}	129	408	130	***86.2***
	10^{-4}	131	406	98	***89.6***
	5. 10^{-4}	134	402	65	***93.1***
	10^{-3}	138	414	36	***96.1***
[OB-IM$^+$, Cl$^-$]	10^{-5}	127	409	154	***83.6***
	5. 10^{-5}	131	407	125	***86.7***
	10^{-4}	134	409	74	***92.1***
	5. 10^{-4}	138	392	48	***94.9***
	10^{-3}	141	417	30	***96.8***

3.4.2. Effect of Temperature

The stability of [OE-IM$^+$, Cl$^-$] and [OB-IM$^+$, Cl$^-$] in molar hydrochloric acid solution with temperature evolution is very crucial for its application. In the present examination, the effect of temperature on the evolution of the corrosion rate and the inhibition inhibitory have been studied within a temperature range of 298K–328 K utilizing potentiodynamic polarization **Figure 8** displays polarization plots for the MS system in 1 M HCl, illustrating changes before and after adding 10^{-3} M of [OE-IM$^+$, Cl$^-$] and [OB-IM$^+$, Cl$^-$] at temperatures from 298K to 328K. In addition, **Table 5** compiles corrosion parameters derived from PDP plots for the [OE-IM$^+$, Cl$^-$] and [OB-IM$^+$, Cl$^-$] systems over a temperature range of 298K to 328K.

From **Figure 8**, increasing the temperature would promote the desorption of both examined compounds and rapid dissolution of MS, thereby weakening the corrosion resistance of MS. The inhibitory efficacy of both inhibitors decreased by increasing the temperature due to the desorption of the adsorbed barrier film of these products onto the MS surface (Shanmugapriya *et al.*, 2023). [OE-IM$^+$, Cl$^-$] and [OB-IM$^+$, Cl$^-$] achieved an inhibitory efficacy of 87.8 % and 89.5%, respectively at 328K. The slight decrease in the inhibitory efficacy of these molecules indicates that these organic species (**Table 5**).

For a comprehensive understanding of the corrosion inhibition mechanism, we assessed the activation energy (E_a), entropy of activation (ΔS_a), and enthalpy of activation (ΔH_a) for MS corrosion in 1 M HCl. This analysis was conducted both before and after the addition of the investigated inhibitors. The Arrhenius equation (19) and its alternative formulation (20) were utilized to derive these parameters. (Didouh *et al.*, 2023; Alaoui Mrani *et al.*, 2021; Larioui *et al.*, 2024):

$$i_{corr} = A\exp\left(-\frac{E_a}{RT}\right) \quad (19)$$

$$\frac{i_{corr}}{T} = \frac{R}{Nh}\exp\left(\frac{\Delta S_a}{R}\right)\exp\left(-\frac{\Delta H_a}{RT}\right) \quad (20)$$

DOI: https://doi.org/10.17509/ijost.v9i2.68764
p- ISSN 2528-1410 e- ISSN 2527-8045

The corrosion rate, indicated by i_{corr}, is influenced by various factors such as absolute temperature (T), Planck's constant (h), Avogadro's number (N), and the molar gas constant (R). **Figure 9** illustrates the Arrhenius plots, depicting ln i_{corr} and ln (i_{corr} /T) versus 1000/T. From these plots, the activation energy (E_a), entropy of activation (ΔH_a), and enthalpy of activation (ΔSa) were derived and are listed in **Table 6**.

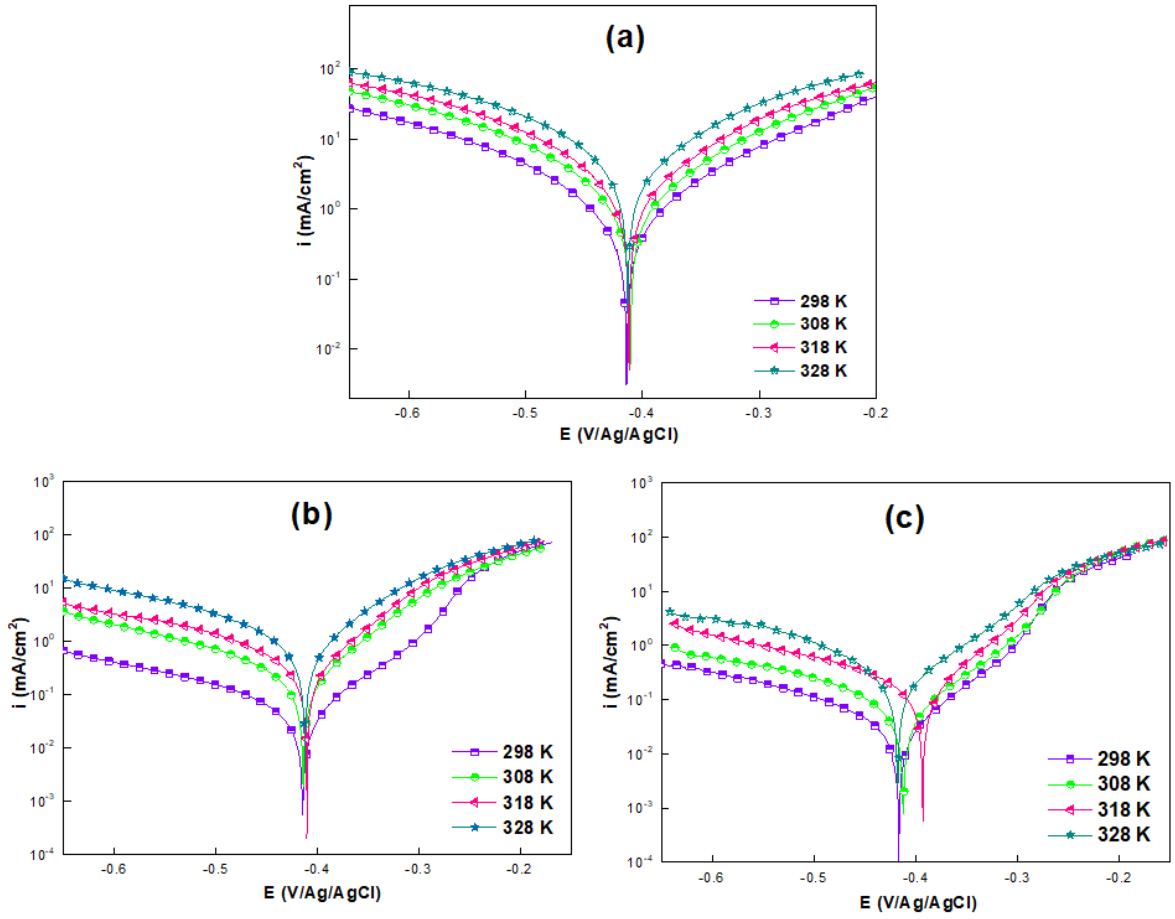

Figure 8. Polarization curves for MS in 1 M HCl **(a)** before and after adding 10^{-3} M of **(b)** [OE-IM$^+$, Cl$^-$] and **(c)** [OB-IM$^+$, Cl$^-$] within a temperature range of 298 K–328 K.

Table 5. Corrosion parameters derived from PDP plots for [OE-IM$^+$, Cl$^-$] & [OB-IM$^+$, Cl$^-$] within a temperature range of 298K–328 K.

Medium	Temperature *(K)*	$-E_{corr}$ *(mV/Ag/AgCl)*	$-\beta_c$ *(Mv/dec)*	i_{corr} *(μA/cm²)*	η_{PDP} *(%)*
Blank	298	413	139	944	--
	308	410	137	1690	--
	318	411	126	2328	--
	328	412	120	3387	--
[OE-IM$^+$, Cl$^-$]	298	414	138	36	***96.1***
	308	413	135	100	***94.0***
	318	410	142	205	***91.2***
	328	412	140	410	***87.8***
[OB-IM$^+$, Cl$^-$]	298	417	141	30	***96.8***
	308	412	146	86	***94.9***
	318	393	143	182	***92.2***
	328	418	133	356	***89.5***

DOI: https://doi.org/10.17509/ijost.v9i2.68764
p- ISSN 2528-1410 e- ISSN 2527-8045

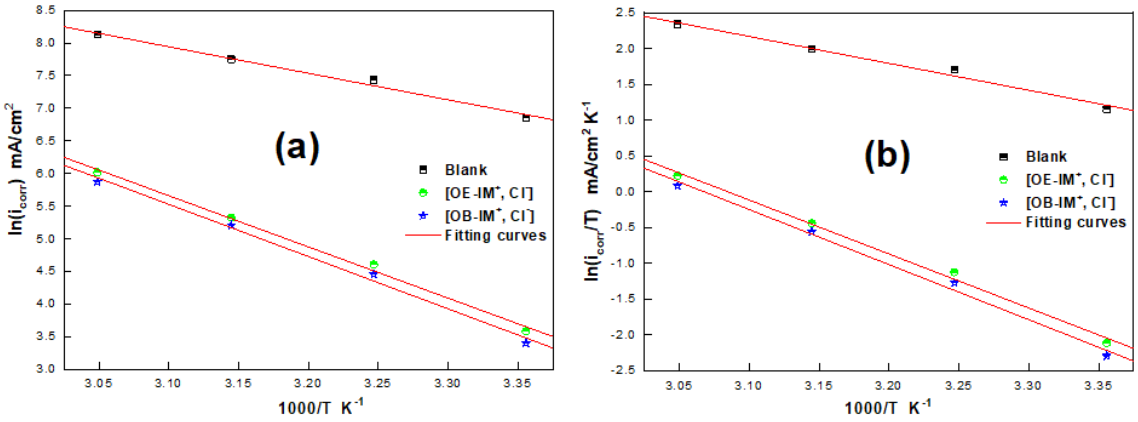

Figure 9. Arrhenius Plots: **(a)** ln i_{corr} vs. 1000/T, **(b)** ln i_{corr} /T vs. 1000/T for MS in 1 M HCl with and without studied ILs.

In this investigation, higher Ea values were observed in the presence of the studied inhibitors compared to those in the 1 M HCl solution alone. This suggests that this behavior may be attributed to physical adsorption onto the steel surface (Alaoui Mrani *et al.*, 2021; Tebbji *et al.*, 2007). Conversely, the large positive values of *ΔHa* reflect the endothermic nature of the MS dissolution process. Furthermore, the increase in the values of *ΔSa* (with lower negative values) in the presence of studied Imidazolium-based ILs compared to the free acid solution implies an increase in order occurring when transitioning from reagents to the steel/solution interface (Salim *et al.*, 2021).

Table 6. Activation parameters for MS in the examined corrosive solution without and with [OE-IM$^+$, Cl$^-$] & [OB-IM$^+$, Cl$^-$].

Medium	Ea (kJ/mol)	ΔHa (kJ/mol)	ΔSa (J/mol.K)
Blank	33.8	31.2	-82.7
[OE-IM$^+$, Cl$^-$]	65.2	62.6	-4.2
[OB-IM$^+$, Cl$^-$]	66.5	63.9	-1.3

3.5. Surface Characterization (SEM-EDS)

The morphological corrosive effects on the MS surface submerged in the investigated corrosive medium before and after adding 10^{-3} M of both examined species after 6 hours of exposure is illustrated in **Figure 10**. Before immersion, it can be seen that the surface of MS was attacked, confirmed by the appearance of pitting, cracks as well as corrosion deposits Figure (10b). Furthermore, the morphology of MS obtained after adding 10^{-3}M of [OE-IM$^+$, Cl$^-$] and [OB-IM$^+$, Cl$^-$] (Figure 10c, d, e) was smoother, more regular and not porous with the appearance of some scratches which can be attributed to the polishing process of MS. These observations highlighted the build-up of a thin barrier film by the organic chemicals that effectively prevents the MS surface from the corrosion process (Chkirate *et al.*, 2021).

The chemical composition of [OE-IM$^+$, Cl$^-$] and [OB-IM$^+$, Cl$^-$] after treatment at 298 K for 6h was investigated utilizing EDS analysis. EDS analysis is reported in **Figure 11**. From **Figure 11**, uninhibited MS EDS spectra show peaks corresponding to some elements that constitute the metal surface. However, inhibited MS EDS shows an additional nitrogen element peak compared to blank (**Figure 11a**). The weight percent composition of the MS surface, as indicated by the spectra, includes 0.65% O, 2.45% C, 0.07% Cl and 96.82 Fe. These data proved the build-up of "iron-oxides "on the metal surface. However, elemental composition recorded with [OE-IM$^+$, Cl$^-$] are 0.22% O, 0.02% Cl, 0.27% N, 2.95% C, and 96.54% Fe and in

DOI: https://doi.org/10.17509/ijost.v9i2.68764
p- ISSN 2528-1410 e- ISSN 2527-8045

the presence of [OB-IM$^+$, Cl$^-$] are 0.57% O, 0.04% Cl, 0.27% N, 1.94% C, and 97.18% Fe. The lower percentage of oxygen (O) detected on the surface of MS compared to the blank spectra indicates a significant reduction in the formation of iron oxide due to the presence of the inhibitor.

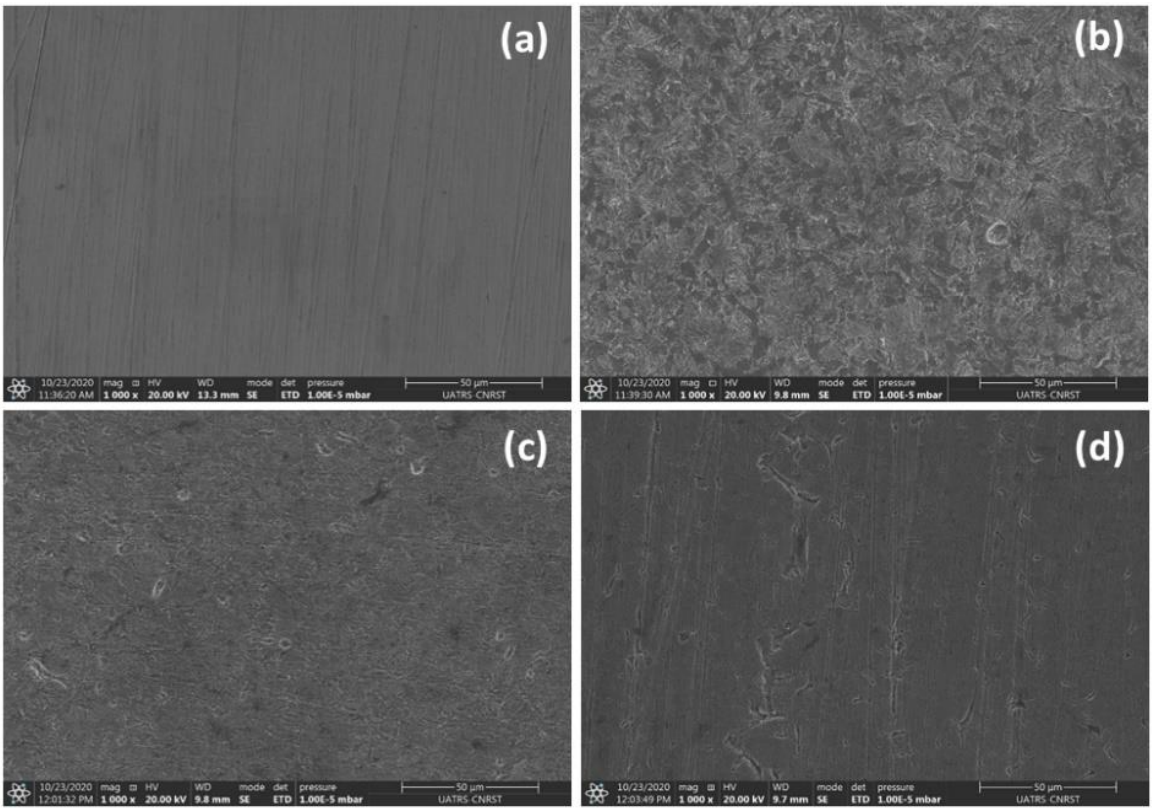

Figure 10. SEM micrographs of MS **(a)** before immersion and after immersion in 1 M HCl **(b)** without inhibitor and with 10-3M of **(c)** [OE-IM$^+$, Cl$^-$] and **(d)** [OB-IM$^+$, Cl$^-$].

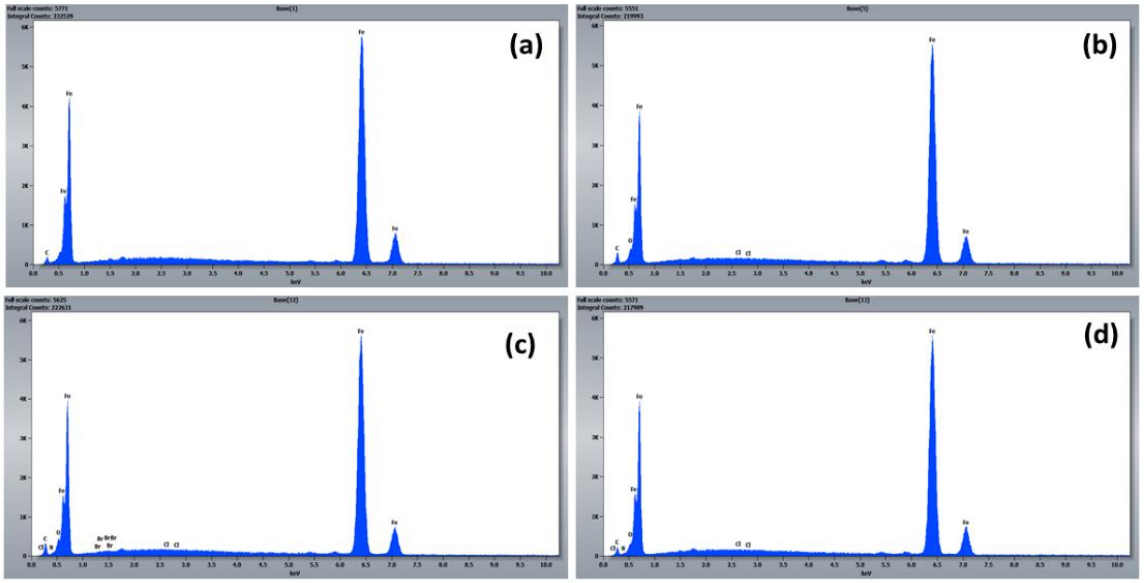

Figure 11. EDS of (a) polished MS surface, (b) MS in 1 M HCl, (c) MS in 1 M HCl after adding 10^{-3}M [OE-IM$^+$, Cl$^-$], and (d) [OB-IM$^+$, Cl$^-$] after 6 h exposure.

DOI: https://doi.org/10.17509/ijost.v9i2.68764
p- ISSN 2528-1410 e- ISSN 2527-8045

3.8. Theoretical Results

3.8.1. DFT calculations

Nowadays, the chemical reactivity tendency, reaction mechanism, and route can be successfully explained by using the FMO analysis, in many scientific fields. In this work, the corrosion inhibition potencies of [OE-IM$^+$, Cl$^-$] and [OB-IM$^+$, Cl$^-$] depicted in the optimized structures in **Figure 12** were investigated by DFT-based reactivity tools. The frontier molecular orbitals (HOMO & LUMO) as well as the molecular electrostatic potential (MEP) plots are presented in **Figure 13**. **Table 7** summarizes the quantum Chemical Parameters of [OE-IM$^+$, Cl$^-$] & [OB-IM$^+$, Cl$^-$] at B3LYP/6-311G (df, pd) level. First, it should be mentioned that both compounds, which are different slightly from each other in terms of the methyl group numbers on the aliphatic chain, tend to react with the "external molecular system" with close affinity. But still, the [OB-IM$^+$, Cl$^-$] molecule preferred to react with the outer molecular system more than the [OE-IM$^+$, Cl$^-$] because the additional two methyl groups on the [OB-IM$^+$, Cl$^-$] with higher flexibility made the interaction easy.

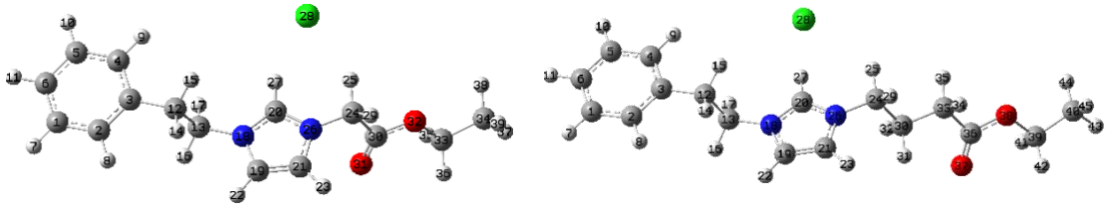

[OE-IM$^+$, Cl$^-$] **[OB-IM$^+$, Cl$^-$]**

Figure 12. Optimized Structures of [OE-IM+, Cl-] & [OB-IM+, Cl-] in the water phase at B3LYP/6-311G (df, pd) Level.

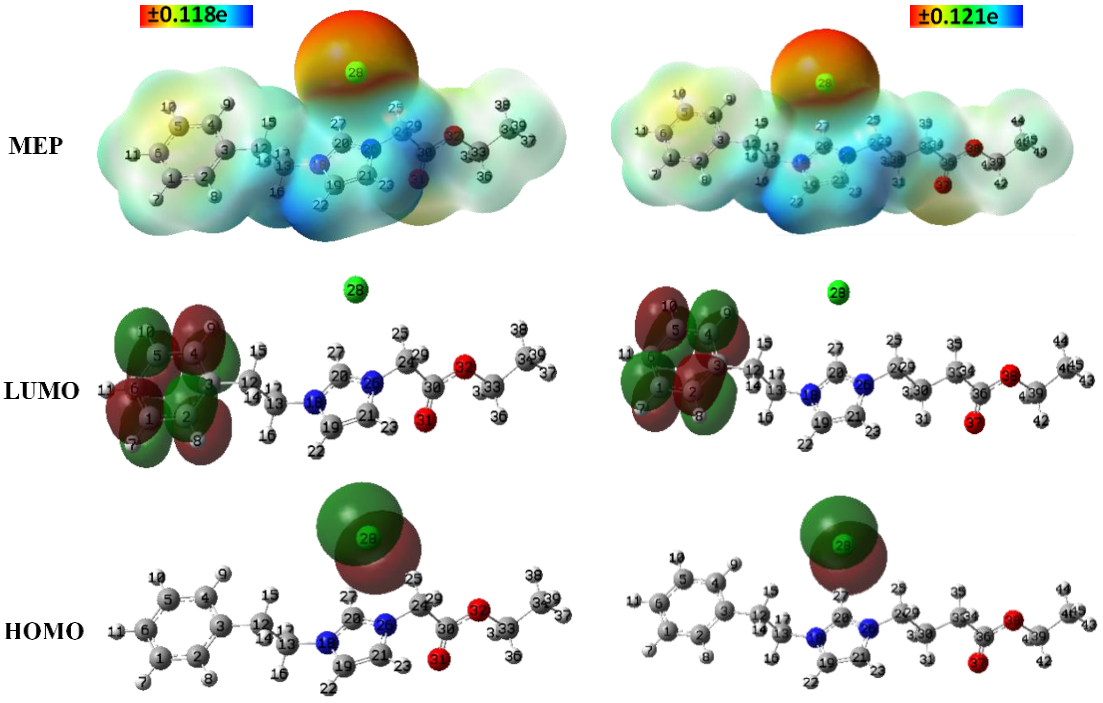

Figure 13. HOMO & LUMO orbitals (isoval:0.02) and MEP (iso value:0.0004) plots of the [OE-IM$^+$, Cl$^-$] & [OB-IM$^+$, Cl$^-$] at B3LYP/6-311G(df, pd) level.

DOI: https://doi.org/10.17509/ijost.v9i2.68764
p- ISSN 2528-1410 e- ISSN 2527-8045

It is well-known that the Koopmans Theorem provides a useful link between Molecular Orbital Theory and Conceptual Density Functional Theory. There is a remarkable correlation between their electron-donating abilities and frontier orbital energy levels of molecules. The molecules with high HOMO orbital energy gives easily the electrons to the steel surface and function effectively as corrosion inhibitors. It is seen from the **Table 7**, [OB-IM$^+$, Cl$^-$] has a higher HOMO energy value than [OE-IM$^+$, Cl$^-$]. LUMO energy represents the electron-accepting capabilities of molecules. The obtained corrosion inhibition efficiency ranking with the help of frontier orbital energies is [OB-IM$^+$, Cl$^-$] > [OE-IM$^+$, Cl$^-$]. This order is in good agreement with experimental observations. Chemical hardness is a property that describes the ability of a molecule to resist the polarization of its electron cloud (Kaya *et al.*, 2015a). As per the Maximum Hardness Principle proposed by Pearson (Kaya *et al.*, 2015b), "There seems to be a rule of nature that molecules arrange themselves to be as hard as possible". According to this principle, η serves as an indicator of stability.

Table 7. Insights into molecular properties: Quantum chemical parameters of [OE-IM+, Cl-] & [OB-IM+, Cl-] at B3LYP/6-311G (df, pd) level.

Component	Gas		Water	
	[OE-IM$^+$, Cl$^-$]	[OB-IM$^+$, Cl$^-$]	[OE-IM$^+$, Cl$^-$]	[OB-IM$^+$, Cl$^-$]
HOMO (-I)	-5.3239	-5.2894	-6.8771	-6.8526
LUMO (-A)	-1.1491	-1.1034	-1.0583	-0.9633
ΔE (L-H)	4.1748	4.1859	5.8189	5.8894
μ	-3.2365	-3.1964	-3.9677	-3.9080
η	2.0874	2.0930	2.9094	2.9447
D (debye)	10.8203	10.4420	17.1179	17.7687
ΔN	0.379	0.388	0.146	0.155
ω	2.5091	2.4408	2.7054	2.5932
ω$^+$	1.1518	1.1042	1.0853	1.0073
ω$^-$	4.3883	4.3006	5.0530	4.9152
Δψ	-0.300	-0.315	-0.062	-0.071
α (au)	199.4667	222.9230	244.2203	272.5927

Ghanty & Ghosh, 1993 noted that chemical softness (the reciprocal of hardness) is directly proportional to the cube root of polarizability. The Minimum Polarizability Principle, proposed within the framework of the Maximum Hardness Principle, posits that polarizability is minimized in a stable state. The η values of the studied molecules are quite similar, but the polarizability value of [OB-IM$^+$, Cl$^-$] is higher than that of [OE-IM$^+$, Cl$^-$]. In light of this data, the corrosion inhibition efficiency can be ranked as follows: [OB-IM$^+$, Cl$^-$] > [OE-IM$^+$, Cl$^-$]. This ranking is consistent with experimental observations. Electronegativity measures a chemical species' ability to withdraw electrons, while electrophilicity, based on absolute hardness and absolute electronegativity, reflects its tendency to accept electrons from electron-rich species. Molecules with higher electronegativity and electrophilicity typically exhibit lower corrosion inhibition effectiveness.

The values in **Table 7** show that electrophilicity and electronegativity values also support the experimental results. The fraction of electrons transferred from the inhibitor molecule to the metal surface serves as a crucial indicator of corrosion inhibition efficiencies. When ΔN > 0, electron transfer occurs from the inhibitor to the metal surface. A higher value of ΔN signifies superior corrosion inhibition performance. Additionally, corrosion inhibitors with more negative metal-inhibitor interaction energy values are typically more effective. With the help of ΔN and Δψ values calculated, we propose inhibition efficiency order as: [OB-IM$^+$, Cl$^-$] > [OE-IM$^+$, Cl$^-$].

DOI: https://doi.org/10.17509/ijost.v9i2.68764
p- ISSN 2528-1410 e- ISSN 2527-8045

These findings align well with the experimental results. For both compounds, the nucleophilic attack site centered on the Cl- ion whereas the LUMO as an electrophilic attack site localized over the aromatic ring. MEP plots also demonstrated that the Cl- ion bore the red color which showed a sign of the electron-rich region the negative electrostatic potential as a function of the total electron density on the molecular structure. In addition, the orange color was seen on the aromatic ring and the oxygen atom of the -C=O group on the aliphatic chain. As expected, the aliphatic -CH_2 group had no responsibility for both the nucleophilic and electrophilic attacks because of the neutral electrostatic potential. Here, it should be recalled that the [OB-IM^+, Cl^-] compound had a more polarizability character than the [OE-IM^+, Cl^-] compound. This property of the two compounds was supported by the electron density value calculated as 0.118e ([OE-IM^+, Cl^-]) <0.121e ([OB-IM^+, Cl^-]).

3.8.2. MD simulation

Molecular dynamics (MD) simulation serves as a valuable tool for investigating the adsorption behavior of the studied inhibitor molecules and identifying their most stable adsorption configurations on the metal surface. By employing the Molecular Dynamics Simulation Approach, adsorption energies can be calculated, providing crucial insights into the corrosion inhibition performances of the molecules. This approach enables a detailed examination of the interactions between the inhibitors and the metal surface, shedding light on the mechanisms underlying their inhibitory effects. **Figure 14** represents the temperature and energy profiles of Investigated ILs/Fe(110) Systems.

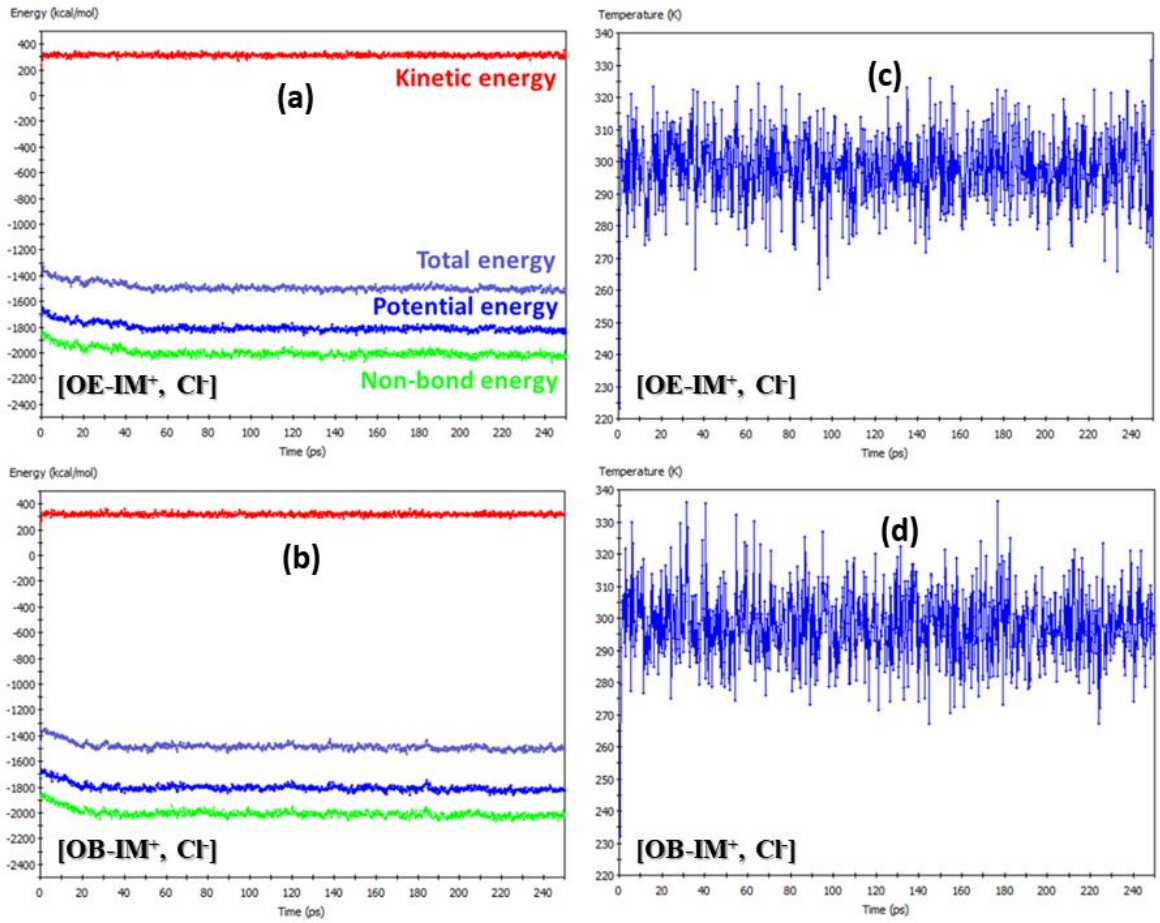

Figure 14. (a,b) Energy profiles and **(c,d)** Temperature of investigated ILs/Fe(110) systems.

DOI: https://doi.org/10.17509/ijost.v9i2.68764
p- ISSN 2528-1410 e- ISSN 2527-8045

Figure 14 illustrates clearly that after 240 picoseconds (ps) of simulation, the temperature and energy profiles have stabilized, indicating that equilibrium has been reached within the studied system. **Figure 15** displays the preferred conformation of the inhibitor molecule adsorbed onto the (110) iron. The molecule adopts a nearly flat orientation on the metal surface, maximizing surface coverage and contact for a strong interaction within the studied ILs/iron system.

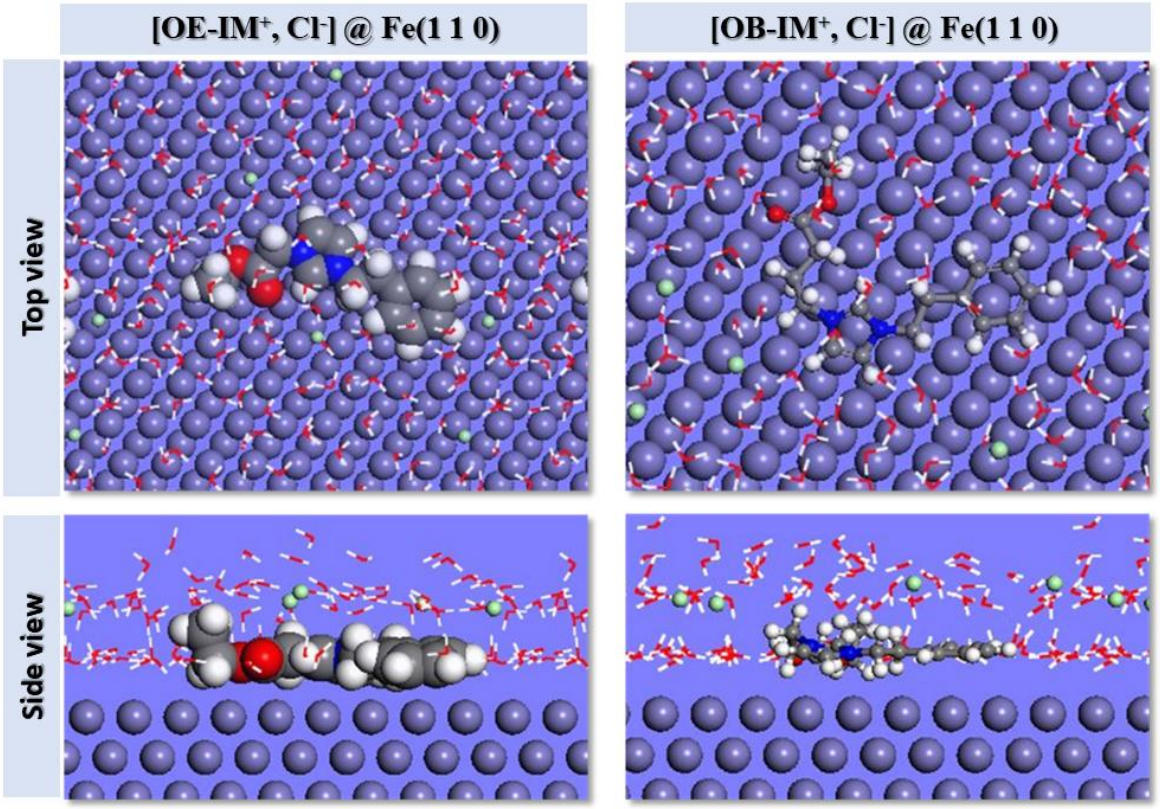

Figure 15. Top and side views for the most stable configuration of **(a)** [OE-IM$^+$, Cl$^-$] and **(b)** [OB-IM$^+$, Cl$^-$] on iron (110) surface.

The computed adsorption energies allow for a comparison of the corrosion inhibition activities of the molecules and provide insights into the interaction between the inhibitor molecule and the metal surface. **Table 8** summarizes the adsorption and binding energies of the investigated inhibitor molecules on the iron surface in a solvated environment. A more negative value of the adsorption energy typically indicates a stronger reactivity between the iron and both studied Ils, suggesting higher corrosion inhibition efficiency (Kokalj *et al.*, 2020; Bourzi *et al.*, 2020). Calculated adsorption energy values for [OE-IM$^+$, Cl$^-$] and [OB-IM$^+$, Cl$^-$] are -176.286 and -201.309 kcal/mol (**Table 8**). It is clear from these data that the interaction between metal surfaces and [OB-IM$^+$, Cl$^-$] is more powerful. For that reason, calculated adsorption energy values also imply that [OB-IM$^+$, Cl$^-$] exhibits greater effectiveness in inhibiting the corrosion of steel compared to [OE-IM$^+$, Cl$^-$].

Table 8. Adsorption and binding energies of investigated inhibitor molecules on iron surface in solvated environment.

Molecule	E_{ads} (kcal/mol)	$E_{Binding}$ (kcal/mol)
[OE-IM$^+$, Cl$^-$]	-176.286	176.286
[OB-IM$^+$, Cl$^-$]	-201.309	201.309

DOI: https://doi.org/10.17509/ijost.v9i2.68764
p- ISSN 2528-1410 e- ISSN 2527-8045

4. CONCLUSION

The investigation focused on assessing the corrosion inhibition efficacy of two newly developed eco-friendly ionic liquid derivatives ([OE-IM$^+$, Cl$^-$] and [OB-IM$^+$, Cl$^-$]) derived from imidazolium, in a 1 M hydrochloric acid solution, for mild steel (MS). The corrosion inhibition properties of both investigated ILs proved to be highly effective against MS in 1 M HCl solution. The inhibition effectiveness of both products increased with higher concentrations but decreased with rising temperatures. At a concentration of 10-3M, the inhibition efficiency of the studied ILs reached 96%, while they still demonstrated very high efficiencies even at elevated temperatures (87-89% at 338K).

Polarization experiments suggest that both imidazolium-based ionic liquid derivatives exhibit a mixed-type inhibition behavior. Electrochemical impedance spectroscopy (EIS) results corroborate these findings, showing an increase in polarization resistance (R_P) and a decrease in double-layer capacitance (C_{dl}) upon the addition of the investigated ILs to 1 M HCl, indicating their effectiveness as corrosion inhibitors. SEM-EDS studies confirm the adsorption of the additive on the metallic surface, following the Langmuir adsorption isotherm. Analysis of the microstructure and chemical composition verifies the formation of a dense film on the MS surface, effectively inhibiting corrosion attack from the medium. DFT calculations were conducted to elucidate the reactivity and reactive sites of both investigated ILs. The results of the DFT analysis effectively explained the inhibition efficiency of these organic compounds. MD simulations further enhanced our understanding of the experimental results, revealing that both molecules adsorb onto the iron surface in a parallel orientation.

5. AUTHORS' NOTE

The authors declare that there is no conflict of interest regarding the publication of this article. The authors confirmed that the paper was free of plagiarism

6. REFERENCES

Abdelshafi, N. S., Farag, A. A., Heakal, F. El-Taib, Badran, A., AbdelAzim, K. M., El Sayed, A.-R. M., Ibrahim, M. A. (2024). In-depth experimental assessment of two new aminocoumarin derivatives as corrosion inhibitors for carbon steel in HCl media combined with AFM, SEM/EDX, contact angle, and DFT/MDs simulations. *Journal of Molecular Structure*, *1304*, 137638.

Alaoui Mrani S., Ech-chihbi E., Arrousse N., Rais Z., El Hajjaji F., El Abiad C., Radi S., Mabrouki J., Taleb M., Jodeh S. (2021). DFT and electrochemical investigations on the corrosion inhibition of mild steel by novel schiff's base derivatives in 1 M HCl Solution. *Arab Journal of Science and Engineering*, *46*, 5691–5707.

Ansari, K. R., Ramkumar, S., Chauhan, D. S., Salman, M., Nalini, D., Srivastava, V., and Quraishi, M. A. (2018). Macrocyclic compounds as green corrosion inhibitors for aluminium: electrochemical, surface and quantum chemical studies. *International Journal of Corrosion and Scale Inhibition*, *7*(3), 443-459.

Ardakani, E. K., Kowsari, E., Ehsani, A. (2020). Imidazolium-derived polymeric ionic liquid as a green inhibitor for corrosion inhibition of mild steel in 1.0 M HCl: Experimental and computational study. *Colloids and Surfaces A: Physicochemical and Engineering Aspects*, *586*, 1241957.

DOI: https://doi.org/10.17509/ijost.v9i2.68764
p- ISSN 2528-1410 e- ISSN 2527-8045

Asfour, H., Elewady, G. Y., Zaki, E. G., and Fouda, A. S. (2023). Synthesis and characterization of new polymeric ionic liquids as corrosion inhibitors for carbon steel in a corrosive medium: Experimental, spectral, and theoretical studies. *CS Omega*, 8(44), 41077–41099.

Asmara Y. P., Kurniawan T., Sutjipto A. G. E., Jafar J. (2018). Application of plants extracts as green corrosion inhibitors for steel in concrete -a review. *Indonesian Journal of Science and Technology*, *3*(2), 158-170.

Azgaou, K., Damej, M., El Hajjaji, S., Sebbar, N. K., Elmselleme, H., El Ibrahimi, B., Benmessaoud, M. (2022). Synthesis and characterization of N-(2-aminophenyl)-2-(5-methyl-1H-pyrazol-3-yl) acetamide (AMPA) and its use as a corrosion inhibitor for C38 steel in 1 M HCl. Experimental and theoretical study. *Journal of Molecular Structure*, *1266*, 133451.

Ben Hmamou, D., Salghi, R., Zarrouk, A., Zarrok, H., Touzani, R., Hammouti, B., El Assyry, A. (2015). Investigation of corrosion inhibition of carbon steel in 0.5 M H_2SO_4 by new bipyrazole derivative using experimental and theoretical approaches. *Journal of Environmental Chemical Engineering*, *3*, 2031–2041.

Benbouguerra K., Chafaa S., Chafai N., Mehri M. (2018). Synthesis, spectroscopic characterization and a comparative study of the corrosion inhibitive efficiency of an α-aminophosphonate and Schiff base derivatives: Experimental and theoretical investigations. *Journal of Molecular Structure*, *1157*, 165–176.

Bouayad, K., Kandri Rodi, Y., El Ghadraoui, E. H., Elmsellem, H., Ouzidan, Y., El Mahi, B., Essassi, E. M., Abdel-Rahman, I., Chetouani, A., Hammouti, B. (2017). Corrosion protection of mild steel in hydrochloric acid at 308 K using benzimidazole derivatives: Weight loss, adsorption and quantum chemical studies. *Moroccan Journal of Chemistry*, *5*(2), 285-296.

Boumhara, K., Tabyaoui, M., Jama, C., and Bentiss, F. (2015). Artemisia mesatlantica essential oil as green inhibitor for carbon steel corrosion in 1 M HCl solution: Electrochemical and XPS investigations. *Journal of Industrial and Engineering Chemistry*, *29*, 146-155.

Bourzi, H., Oukhrib, R., El Ibrahimi, B., AbouOualid, H., Abdellaoui, Y., Balkard, B., Hilali, M., and El Issami, S. (2020). Understanding of anti-corrosive behavior of some tetrazole derivatives in acidic medium: Adsorption on Cu (111) surface using quantum chemical calculations and Monte Carlo simulations. *Surface Science*, *702*, 121692.

Chkirate, K., Azgaou, K., Elmsellem, H., El Ibrahimi, B., Sebbar, N. K., Anouar, E. H., Benmessaoud, M., El Hajjaji, S., Essassi, E. M. (2021). Corrosion inhibition potential of 2-[(5-methylpyrazol-3-yl)methyl] benzimidazole against carbon steel corrosion in 1 M HCl solution: Combining experimental and theoretical studies. *Journal of Molecular Liquids*, *321*, 114750.

Cris, C. A., Timis, E. C., Vermes, H. (2023). PickT: A decision-making tool for the optimal pickling process operation. *Materials*, *16*, 5567.

DOI: https://doi.org/10.17509/ijost.v9i2.68764
p- ISSN 2528-1410 e- ISSN 2527-8045

Deng, Q., Jeschke, S., Mishra, R. K., Spicher, S., Darouich, S., Schreiner, E., Eiden, P., Deglmann, P., Gorges, J. N., Chen, X.-B., Keil, P., Cole, I. (2024). Design of alkyl-substituted aminothiazoles to optimize corrosion inhibition for galvanized steel: A combined experimental and molecular modeling approach. *Corrosion Science*, *227*, 111733.

Didouh, H., Buyuksagis, A., Meliani, M. H., Dilek, M., Kayali, Y., Suleiman, R. K., Saleh, T. A. (2023). Investigating the use of moringa oleifera leaf extract as an environment-friendly corrosion inhibitor for API 5L X52 steel in 1 M HCl. *Journal of Molecular Liquids*, *390*, 122910.

Ech-chihbi, E., Salim, R., Ouakki, M., Koudad, M., Guo, L., Azam, M., Benchat, N., Rais, Z., Taleb, M. (2023). Corrosion resistance assessment of copper, mild steel, and aluminum alloy 2024-T3 in acidic solution by a novel imidazothiazole derivative. *Materials Today Sustainability*, 24, 100524.

Ech-chihbi, E., Salim, R., Oudda, H., Elaatiaoui A., Rais Z., Oussaid A., El Hajjaji F., Hammouti B., Elmsellem H., Taleb M. (2016). Effect of some imidazopyridine compounds on carbon steel corrosion in hydrochloric acid solution. Der Pharm Chem, 8(13), 214-230.

El Faydy M., Touir R., Touhami M. E., Zarrouk A., and Jama C. (2018). Corrosion inhibition performance of newly synthesized 5-alkoxymethyl-8-hydroxyquinoline derivatives for carbon steel in 1 M HCl solution: Experimental, DFT and Monte Carlo simulation studies. *Physical Chemistry Chemical Physics*, *20*, 20167.

El-Hajjaji, F., Ech-chihbi, E., Rezki, N., Benhiba, F., Taleb, M., Chauhan, D. S., Quraishi, M. A. (2020). Electrochemical and theoretical insights on the adsorption and corrosion inhibition of novel pyridinium-derived ionic liquids for mild steel in 1 M HCl. *Journal of Molecular Liquids*, *314*, 113737.

El-khlifi, A., Zouhair, F. Z., Lgaz, H., Saadouni, M., Salghi, R., Merimi, I., Siaj, M., and Erramli, H. (2024). Evaluation of 1, 4-benzothiazines in steel corrosion inhibition in 15% hcl: experimental and theoretical perspectives. *Moroccan Journal of Chemistry*, *12*(2), 509-533.

El-Nagar, R. A., Khalil, N. A., Atef, Y. (2024). Evaluation of ionic liquids based imidazolium salts as an environmentally friendly corrosion inhibitors for carbon steel in HCl solutions. *Scientific Reports*, *14*, 1889.

Feng, L., Zhang, S., Qiang, Y., Xu, S., Tan, B., Chen, S. (2018). The synergistic corrosion inhibition study of different chain lengths ionic liquids as green inhibitors for X70 steel in acidic medium. *Materials Chemistry and Physics*, *215*, 229-241.

Gadioli, A. O., de Souza, L. M., Pereira, E. C., Monteiro, S. N., Azevedo, A. R. G. (2024). Imidazolium-based ionic liquids as corrosion inhibitors for stainless steel in different corrosive media: An overview. *Journal of Materials Research and Technology*, *29*, 803–823.

Gazquez, J. L., Cedillo, A., and Vela, A. (2007). Electrodonating and electroaccepting powers. The *Journal of Physical Chemistry A*, *111*(10), 1966-1970.

DOI: https://doi.org/10.17509/ijost.v9i2.68764
p- ISSN 2528-1410 e- ISSN 2527-8045

Ghanty, T. K., and Ghosh, S. K. (1993). Correlation between hardness, polarizability, and size of atoms, molecules, and clusters. *The Journal of Physical Chemistry*, *97*(19), 4951-4953.

Ghazoui, A., Bencaht, N., Al-Deyab, S. S., Zarrouk, A., Hammouti, B., Ramdani, M., Guenbour, M. (2013). An investigation of two novel pyridazine derivatives as corrosion inhibitors for C38 Steel in 1.0 M HCl. *International Journal of Electrochemical Science*, *8*, 2272–2292.

Ghiaty, E. A., Shafek, S. H., and Atta, A. M. (2024). Morphological performances and corrosion inhibition mechanism of new amphiphilic tetra-cationic imidazolium ionic liquids for carbon steel in 1 M HCl medium. *Journal of Molecular Structure*, *1300*, 137252.

Goyal, M., Vashisht, H., Kumar, A., Kumar, S., Bahadur, I., Benhiba, F., Zarrouk, A. (2020). Isopentyltriphenylphosphoniumbromideionic liquid as a newly effective corrosion inhibitor on metal-electrolyte interface in acidic medium: Experimental, surface morphological (SEM-EDX and AFM) and computational analysis. *Journal of Molecular Liquids*, *316*, 113838.

Hamani, H., Douadi, T., Al-Noaimi, M., Issaadi, S., Daoud, D., Chafaa, S. (2014). Electrochemical and quantum chemical studies of some azomethine compounds as corrosion inhibitors for mild steel in 1 M hydrochloric acid. *Corrosion Science*, *88*, 234-245.

Haque, J., Verma, C., Srivastava, V., Wan Nik, W. B. (2021). Corrosion inhibition of mild steel in 1 M HCl using environmentally benign Thevetia peruviana flower extracts. *Sustainable Chemistry and Pharmacy*, *19*, 100354.

Hrimla, M., Bahsis, L., Boutouil, A., Laamari, M. R., Julvec, M., Stiriba, S. (2021). Corrosion inhibition performance of a structurally well-defined 1,2,3-triazole derivative on mild steel-hydrochloric acid interface. *Journal of Molecular Structure*, *1231*, 129895.

Huang, L., Yang, K.-P., Zhao, Q., Li, H.-J., Wang, J.-Y., Wu, Y.-C. (2022). Corrosion resistance and antibacterial activity of procyanidin B2 as a novel environment-friendly inhibitor for Q235 steel in 1 M HCl solution. *Bioelectrochemistry*, *143*, 107969.

Jalab, R., Saad, M., Benali, A., Hussein, I. A., Khaled, M. (2023). Biodegradable polysaccharide grafted polyacrylamide inhibitor for corrosion in CO2-saturated saline solution. *Heliyon*, *9*, e20304.

Ji, Y., Xu, B., Gong, W., Zhang, X., Jin, X., Ning, W., Meng, Y., Yang, W., Chen, Y. (2016). *Journal of the Taiwan Institute of Chemical Engineers*, *66*, 301.

Kaya, S., and Kaya, C. (2015a). A new equation for calculation of chemical hardness of groups and molecules. *Molecular Physics*, *113*(11), 1311-1319.

Kaya, S., and Kaya, C. (2015b). A simple method for the calculation of lattice energies of inorganic ionic crystals based on the chemical hardness. *Inorganic Chemistry*, *54*(17), 8207-8213.

DOI: https://doi.org/10.17509/ijost.v9i2.68764
p- ISSN 2528-1410 e- ISSN 2527-8045

Kokalj, A., Behzadi, H., and Farahati, R. (2020). DFT study of aqueous-phase adsorption of cysteine and penicillamine on Fe(110): Role of bond-breaking upon adsorption. *Applied Surface Science*, *514*, 145896.

Larioui, A., Hmada, A., El Magri, A., Errahmany, N., El Hajri, F., Dkhireche, N., El Bakkali, S., Touir, R., and Boukhris, S. (2024). Corrosion inhibition influence of the synthetized chromen-6-one derivatives on mild steel in 1.0 M HCl electrolyte: Electrochemical, spectroscopic and theoretical investigations. *Moroccan Journal of Chemistry*, *12*(2), 570-593.

Lazrak, J., Ech-chihbi, E., El Ibrahimi, B., El Hajjaji, F., Rais, Z., Tachihante, M., Taleb, M. (2022). Detailed DFT/MD simulation, surface analysis and electrochemical computer explorations of aldehyde derivatives for mild steel in 1.0 M HCl. *Colloids and Surfaces A: Physicochemical and Engineering Aspects, 632*, 127822.

Li, E., Liu, S., Luo, F., and Yao, P. (2023). Amino acid imidazole ionic liquids as green corrosion inhibitors for mild steel in neutral media: Synthesis, electrochemistry, surface analysis and theoretical calculations. *Journal of Electroanalytical Chemistry*, *944*, 117650.

Mangalam, N. A., Kurup, M. P., Suresh, E., Kaya, S., and Serdaroğlu, G. (2021). Diversities in the chelation of aroylhydrazones towards cobalt (II) salts: Synthesis, spectral characterization, crystal structure and some theoretical studies. *Journal of Molecular Structure*, *1232*, 129978.

Murmu, M., Saha, S. K., Murmu, N. C., Banerjee, P. (2019). Effect of stereochemical conformation into the corrosion inhibitive behaviour of double azomethine based Schiff bases on mild steel surface in 1 mol L−1 HCl medium: an experimental, density functional theory and molecular dynamics simulation study. *Corrosion Science*, *146*, 134-151.

Njoku, A. C., Anyanwu, P. I., and Nwanonenyi, S. C. (2023). Understanding the anticorrosion properties of chitosan grafted poly-aspartic acid against mild steel corrosion in 1 M HCl: Electrochemical and theoretical considerations. *Moroccan Journal of Chemistry*, *11*(04), 11-4.

Olivares, Z. G., Hernández Gayosso, M. J., and Mora Mendoza, J. L. (2007). Corrosion inhibitors performance for mild steel in CO2 containing solutions. *Materials and Corrosion*, *58*(6), 427-437.

Ouakki, M., Galai, M., Benzekri, Z., Arribou, Z., Ech-chihbi, E., Guo, L., Dahmani, K., Nouneh, K., Briche, S., Boukhris, S., Cherkaoui, M. (2021). A detailed investigation on the corrosion inhibition effect of newly synthesized Pyran derivative on mild steel in 1.0 M HCl: Experimental, surface morphological (SEM-EDS, DRXand AFM) and computational analysis (DFT and MD simulation). *Journal of Molecular Liquids*, *344*, 117777.

Ouakki, M., Galai, M., Rbaa, M., Abousalem, A. S., Lakhrissi, B., EbnTouhami, M., Cherkaoui, M. (2020). Electrochemical, thermodynamic and theoretical studies of some imidazole derivatives compounds as acid corrosion inhibitors for mild steel. *Journal of Molecular Liquids*, *319*, 114063.

DOI: https://doi.org/10.17509/ijost.v9i2.68764
p- ISSN 2528-1410 e- ISSN 2527-8045

Parr, R. G., Szentpály, L. V., and Liu, S. (1999). Electrophilicity index. *Journal of the American Chemical Society*, *121*(9), 1922-1924.

Preethi Kumari, P., Shetty, P., and Rao, S. A. (2017). Electrochemical measurements for the corrosion inhibition of mild steel in 1 M hydrochloric acid by using an aromatic hydrazide derivative. *Arabian Journal of Chemistry*, *10*(5), 653–663.

Rajeswari, V., Kesavan, D., Gopiraman, M., Viswanathamurthi, P., Poonkuzhali, K., Palvannan, T. (2014). Corrosion inhibition of Eleusine aegyptiaca and Croton rottleri leaf extracts on cast iron surface in 1 M HCl medium. *Applied Surface Science*, *314*, 537-545.

Rochdi, A., Kassou, O., Dkhireche, N., Touir, R., El Bakri, M., Touhami, M. E., Sfaira, M., Mernari, B., Hammouti, B. (2014). Inhibitive properties of 2,5-bis(n-methylphenyl)-1,3,4-oxadiazole and biocide on corrosion, biocorrosion and scaling controls of brass in simulated cooling water. *Corrosion Science*, *80*, 442-452.

Salim, R., Nahlé, A., El-Hajjaji, F., Ech-chihbi, E., Benhiba, F., El Kalai, F., Benchat, N., Oudda, H., Guenbour, A., Taleb, M., Warad, I., Zarrouk, A. (2021). Experimental, density functional theory, and dynamic molecular studies of imidazopyridine derivatives as corrosion inhibitors for mild steel in hydrochloric acid. *Surface Engineering and Applied Electrochemistry*, *57*(2), 233–254.

Serdaroğlu, G., Kaya, S., and Touir, R. (2020). Eco-friendly sodium gluconate and trisodium citrate inhibitors for low carbon steel in simulated cooling water system: Theoretical study and molecular dynamic simulations. *Journal of Molecular Liquids*, *319*, 114108.

Shanmugapriya, R., Ravi, M., Ravi, S., Ramasamy, M., Maruthapillai, A., Selvi, J. A. (2023). Electrochemical and morphological investigations of elettaria cardamomum pod extract as a green corrosion inhibitor for mild steel corrosion in 1 N HCl. *Inorganic Chemistry Communications*, *154*, 110958.

Sheetal, A., Singh, A. K., Thakur, S., Pani, B., Singh, M. (2024). Heterocyclic compounds as corrosion inhibitors for iron alloys in various industrial processes: A review. *Journal of Industrial and Engineering Chemistry*, *130*, 141–177.

Singh, A. K., Chugh, B., Singh, M., Thakur, S., Pani, B., Guo, L., and Serdaroglu, G. (2021). Hydroxy phenyl hydrazides and their role as corrosion impeding agent: A detailed experimental and theoretical study. *Journal of Molecular Liquids*, *330*, 115605.

Souza, L., Pereira, E., Matlakhova, L., Nicolin, V. A. F., Monteiro, S. N., de Azevedo, A. R. G. (2023). Ionic liquids as corrosion inhibitors for carbon steel protection in hydrochloric acid solution: A first review. *Journal of Materials Research and Technology*, *22*, 2186–2205.

Tebbji, K., Bouabdellah, I., Aouniti, A., Hammouti, B., Oudda, H., Benkaddour, M., and Ramdani, A. (2007). N-benzyl-N, N-bis [(3, 5-dimethyl-1H-pyrazol-1-yl) methyl] amine as corrosion inhibitor of steel in 1 M HCl. *Materials Letters*, *61*(3), 799-804.

Udunwa, D. I., Onukwuli, O. D., Nwanonenyi, S. C., Ezekannagha, C. B. (2024). Novel imidazole based ionic liquid as anti-corrosion additive for aluminum alloy: Combined experimental,

DOI: https://doi.org/10.17509/ijost.v9i2.68764
p- ISSN 2528-1410 e- ISSN 2527-8045

DFT/MD simulation and soft computing approach. *Applied Surface Science Advances*, *19*, 100578.

Zarrouk, A., Messali, M., Zarrok, H., Salghi, R., Al-Sheikh Ali, A., Hammouti, B., Al-Deyab, S.S. Bentiss, F. (2012). Synthesis, characterization and comparative study of new functionalized imidazolium-based ionic liquids derivatives towards corrosion of c38 steel in molar hydrochloric acid. *International Journal of Electrochemical Science, 7*(8), 6998-7015.

Zerga B., Attayibat A., Sfaira M., Taleb M., Hammouti B., Ebn Touhami M., Radi S., Rais Z. (2010), Effect of some tripodal bipyrazolic compounds on C38 steel corrosion in hydrochloric acid solution. *Journal of Applied Electrochemistry, 40*(9), 1575-1582

Zhang, G. A., Hou, X. M., Hou, B. S., Liu, H. F. (2019). Benzimidazole derivatives as novel inhibitors for the corrosion of mild steel in acidic solution: Experimental and theoretical studies. *Journal of Molecular Liquids*, *278*, 413–422.

DOI: https://doi.org/10.17509/ijost.v9i2.68764
p- ISSN 2528-1410 e- ISSN 2527-8045